Fault Contributions From Inverter-Based Resources: Field Insights and Protection Challenges

Mukesh Nagpal
Burns & McDonnell

Ajmal Saeed, Ricardo Rangel, and Daniel Zhang
Pacific Gas & Electric Company

Ritwik Chowdhury
Schweitzer Engineering Laboratories, Inc.

Presented at the
52nd Annual Western Protective Relay Conference
Spokane, Washington
October 28–30, 2025

Fault Contributions From Inverter-Based Resources: Field Insights and Protection Challenges

Mukesh Nagpal, *Burns & McDonnell*
Ajmal Saeed, Ricardo Rangel, and Daniel Zhang, *Pacific Gas & Electric Company*
Ritwik Chowdhury, *Schweitzer Engineering Laboratories, Inc.*

Abstract—The growing penetration of inverter-based resources (IBRs), including solar photovoltaics, wind turbines, and battery energy storage systems, is reshaping modern transmission grids and introducing complex protection challenges. These challenges arise from IBRs' limited short-circuit current contributions, unpredictable magnitudes and phase angles of negative-sequence currents under unbalanced conditions, and non-deterministic control responses during faults, system disturbances, and even steady-state operations.

Traditional protection schemes, developed for synchronous machines with high inertia, predictable fault behavior, and largely clean voltage and current waveforms during steady-state operation, are increasingly inadequate in environments with high penetration of IBRs. This paper presents approximately 30 field-recorded events that illustrate these vulnerabilities, including misoperation of directional and distance elements, instability of memory-polarized logic, reactive current discontinuities risking inadvertent breaker failure, and resonant or oscillatory phenomena involving IBR controls.

The findings underscore the need to adapt protection philosophies to reflect the software-defined and fast-acting nature of IBR controls. This paper provides practical insights for protection engineers, utilities, and manufacturers, while emphasizing the importance of multidisciplinary collaboration to ensure dependable, secure, and selective protection in the evolving grid landscape.

I. Introduction

For over a century, power system protection schemes have been designed around the predictable behavior of synchronous generators, where fault response is governed by physical inertia and robust short-circuit current contributions. These schemes rely heavily on phasor-based measurements and deterministic angular relationships between voltages and currents to ensure dependable fault detection, discrimination, and coordination.

The increasing penetration of inverter-based resources (IBRs), including solar photovoltaic (PV), battery energy storage systems (BESSs), and wind turbine generators (WTGs), is fundamentally altering this paradigm. Unlike synchronous machines, IBRs interface with the grid through power-electronic converters, whose fault responses are dictated not by the physical construction but rather by fast-acting control algorithms. These algorithms prioritize equipment protection and often impose strict limits on fault current magnitude, duration, and phase angle. Under unbalanced voltage conditions, many IBRs inject little to no negative-sequence current, and when they do, the angular relationships with sequence voltages and currents are often erratic or non-deterministic, posing serious challenges to traditional protection logic.

This paper investigates these emerging protection challenges through the lens of approximately 30 unique real-world disturbance records spanning 25 years collected from diverse IBR installations. These events reveal the limitations of conventional phasor-based protection approaches when applied to modern grids with a high penetration of IBRs.

- **Section II** provides an overview of IBR technologies.
- **Section III** provides an overview of line protection practices referenced in the events of this paper.
- **Section IV** highlights transmission line protection challenges, including unreliable directional element performance, misidentification of faulted phases during ground faults, unpredictable dynamic expansion of memory-polarized distance relay characteristics, false assertion of a loss-of-potential due to controlled current limiting, and risks of out-of-synchronism reclosing.
- **Section V** examines IBR cease-mode behavior and its variations, which introduce significant reliability concerns for protection schemes.
- **Section VI** addresses overvoltage protection and frequency measurement challenges, particularly in scenarios involving inadvertent islanding and high rate-of-change-of-frequency (ROCOF) conditions.
- **Section VII** investigates transformer overexcitation and broader system-level risks such as subsynchronous oscillations (SSOs).
- **Section VIII** analyzes IBR harmonics and their impact on power quality, protection reliability, and potential breaker failure scenarios.
- **Section IX** highlights unanticipated control interactions within IBRs, including self-excited current oscillations and dynamic instability without clear initiating events.
- **Section X** presents a summary table to aid the reader in navigating to the different field events in this paper.
- **Section XI** consolidates key observations and proposes practical countermeasures to improve protection reliability.

This paper does not claim to provide definitive solutions to the diverse and evolving protection challenges posed by IBRs. Rather, its objective is to present real-world insights, contrasting the model-driven focus of existing literature, to

illuminate the nature and complexity of these issues. Many of the cases analyzed reflect conditions not fully captured in conventional planning studies or compliance simulations.

Ultimately, achieving reliable protection in an IBR-dominated grid will require collaborative innovation across multiple domains. Meaningful progress hinges on deeper visibility into IBR control logic, proactive updates to regulatory frameworks, and the development of adaptive protection schemes that account for the dynamic, software-defined nature of modern power generation.

II. Classification of IBRs

IBRs can be classified based on their power-electronic interface or control strategy. The interface and control strategy significantly influences their current output during faults.

A. Partial Converter-Interfaced IBRs

The partial converter interface is used in Type III wind generators, which employ doubly fed induction generators (DFIGs). Fig. 1 illustrates the block diagram of this configuration. The turbine drives the DFIG, which has rotor windings excited by an alternating current (ac) source of variable magnitude and frequency. The stator windings directly connect to the grid at power frequency. The rotor windings interface with the grid through partially rated power-electronic converters. This arrangement allows for the supply of variable slip frequency current to the rotor, thereby accommodating changing wind conditions.

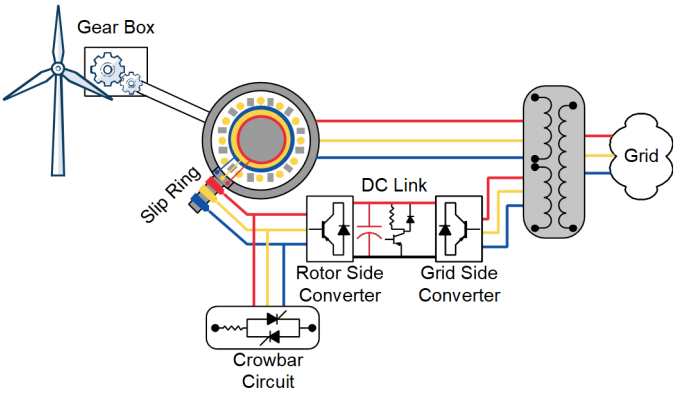

Fig. 1. Type III WTG with partial converter interface

B. Full Converter-Interfaced IBRs

Solar, BESSs, and Type IV WTGs connect to the grid through fully rated power-electronic converters, often called full converters or simply inverters. Fig. 2 illustrates the basic configuration. These converters transform the sources' direct current (dc) or variable-frequency ac voltage into grid-synchronized, power-frequency ac voltage. Fully rated converters are more expensive than the partial converters and introduce higher losses.

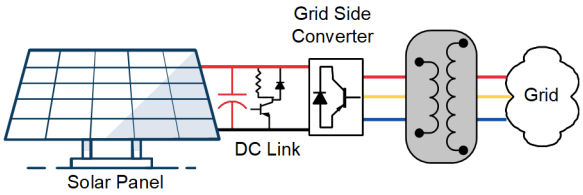

Fig. 2. Solar PV with full converter interface

C. Grid-Following (GFL) Versus Grid-Forming (GFM) IBRs

Most IBR installations connected to transmission systems today use grid-following control systems. They have a built-in phase-locked loop (PLL) that locks to the grid voltage and a self-synchronizing controller to align their output with the grid. A resource with grid-following control cannot operate independently after disconnection from the grid or in the event of a grid outage.

Nearly all initial installations of renewable resources employing grid-following control were designed to inject balanced or positive-sequence current (I_1) while retaining their active power output at their respective set points. However, new grid codes and standards are increasingly requiring the injection of negative-sequence current (I_2) during unbalanced faults [1] [2]. This requirement aims for IBRs to mimic the fault current behavior of synchronous generators during both balanced and unbalanced faults. Despite this division between I_1 and I_2 injection requirements, the total phase current during a fault typically remains limited to 1.0 to 1.3 pu of the IBR's rated current. This limitation stems from the power-electronic converter ratings.

Grid-following control systems do not address load-generation mismatches, which can undermine grid stability under high penetration of IBRs. To address these limitations, grid-forming control systems have been introduced. Drawing upon decades of experience with grid-forming controls in microgrids and islanded power systems, grid-forming controls enable converters to independently establish and regulate grid voltage and frequency. Currently, their penetration at transmission voltage levels is limited, and related events are not included in this paper.

III. Line Protection Overview

This section provides a refresher on phasor-based protection functions used to design present-day protective relays intended for systems with synchronous generation sources. It focuses on three functions commonly used in networked transmission lines: directional elements, faulted phase identification logics, and memory-polarized mho distance elements.

A. Directional Element

In networked transmission lines, directional elements determine whether a fault is in front of or behind the relay location. This facilitates selective tripping by helping to minimize the affected outage area. As illustrated in Fig. 3, the angular relationship between I_2 and I_0 phasors with respect to their corresponding negative-sequence voltage (V_2) and zero-sequence voltage (V_0) phasors measured at the relay location can be used to determine fault direction.

When the sequence current leads the corresponding voltage by approximately 90 degrees, the fault is identified as being in front of the relay, i.e., in the forward direction. Conversely, if the sequence current lags the corresponding voltage by about 90 degrees, the fault is behind the relay, i.e., in the reverse direction. This angular relationship assumes an inductive path from the source to the fault location, which governs the phase shift between current and voltage under fault conditions.

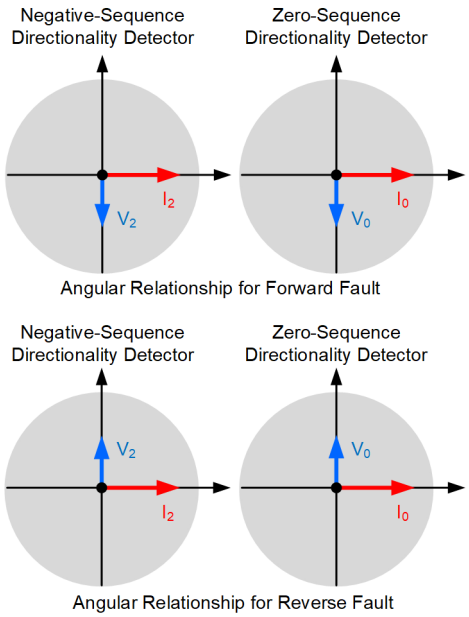

Fig. 3. Angular relationship used by negative- and zero-sequence directional elements

In legacy electromechanical relays, zero-sequence directional elements were commonly used for ground fault directionality due to the simplicity of implementing the zero-sequence filter by summing the three-phase currents or voltages. Negative-sequence directional elements offered several advantages:

- Immunity to incorrect directional decisions in lines with zero-sequence mutual coupling
- Higher sensitivity to high-resistance faults
- Applicability to all unbalanced faults, including phase-to-phase faults (in addition to ground faults)

However, they were not widely adopted due to the complexity and cost of implementing negative-sequence filtering in legacy relay technology.

With the advent of microprocessor-based relays, implementing negative-sequence filtering became simple. As a result, the use of negative-sequence directional elements has become widespread [3]. In many applications, relay manufacturers and protection engineers now use negative-sequence directional elements to supervise distance and fault detection elements, particularly for selective tripping during unbalanced faults.

For the events presented in this paper, the negative-sequence directional (32Q) element determines fault direction by calculating the negative-sequence impedance, Z_2 [4]. The simplified logic implementation of the 32Q element is represented in Fig. 4. If sufficient I_2 is available, 32QE asserts and Z_2 is calculated. The Z_2 is then compared with forward and reverse impedance thresholds (see Fig. 5) to declare a forward fault (32QF) or reverse fault (32QR). Similar logic is used for the zero-sequence directional element (32V). When sufficient I_0 is available, 32VE asserts and Z_0 calculations are enabled to declare either a forward (F32V) or reverse (R32V) fault.

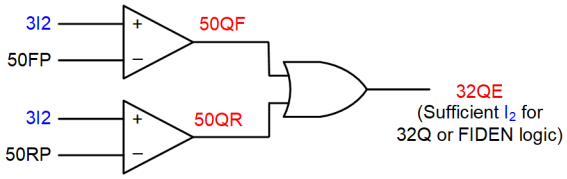

Fig. 4. Negative-sequence enable logic for directional and faulted phase identification logic

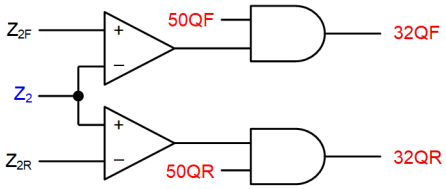

Fig. 5. Negative-sequence directional logic

B. Faulted Phase Identification

Microprocessor-based relays include built-in faulted phase identification logic that helps prevent an overreach of unfaulted distance loops. These algorithms also aid single-phase tripping, fault location, and targeting.

One commonly used method for faulted phase identification for ground faults involves using the angular relationship between I_2 and I_0 [5]. Fig. 6 illustrates this approach (using Phase A as a reference):

- I_2 in-phase with I_0 indicates an AG or BCG fault
- I_2 lagging I_0 by 120 degrees denotes a BG or CAG fault
- I_2 leading I_0 by 120 degrees corresponds to a CG or ABG fault

The gray areas in Fig. 6 represent tolerances used by this current-based scheme to account for nonhomogeneity between the negative- and zero-sequence networks and measurement errors. This approach assumes the following response from the source, which is typical of synchronous generators:

- A stable source frequency
- Inductive source impedance

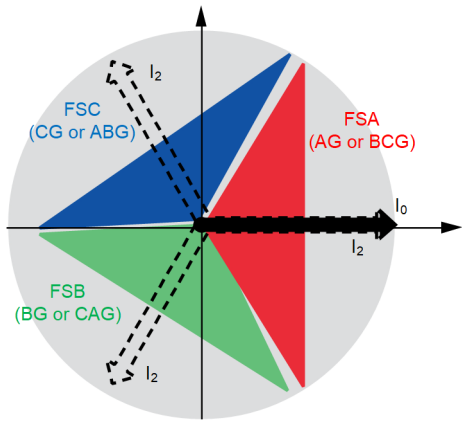

Fig. 6. Angular relationship of negative-sequence current with respect to zero-sequence current for faulted phase identification

Over time, it was observed that the current-based scheme is not dependable in systems that are weak in the positive- and negative-sequence networks and are strong in the zero-sequence network (e.g., near a large, grounded power transformer) [6]. In such systems, voltages can be used to supplement the current-based scheme previously discussed. One implementation is shown in Fig. 7 [7]. If there is both sufficient I_2 (32QE asserts) and I_0 (32VE asserts), the angle between I_2 and I_0 is used. Otherwise, for a weak-infeed application, the undervoltage algorithm can be used for faulted phase identification.

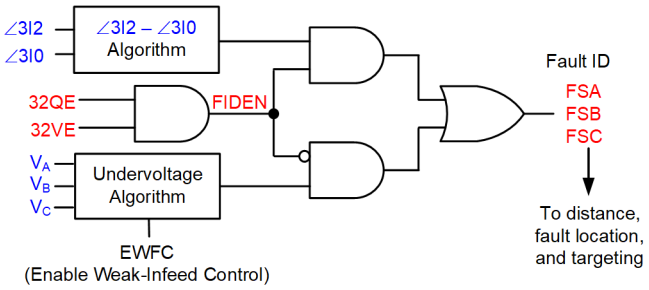

Fig. 7. Faulted phase identification logic using currents and voltages

The events discussed in this paper only use the current-based faulted phase identification logic.

C. *Memory-Polarized Mho Distance Element*

The mho element is one of the most widely used functions in networked transmission line protection. It determines the distance to a fault by calculating the apparent impedance from the relay location to the fault. The element is inherently directional, relying on system voltage as a polarizing signal to determine whether the fault is forward (in the protected zone) or reverse (behind the relay).

During a three-phase fault at or very close to the relay location, the polarizing signal (i.e., the voltage at the relay terminal) collapses, rendering the relay unable to make a directional decision. To overcome this limitation, modern relays use the pre-fault voltage, stored in memory, for polarization [8].

Under normal (steady-state) conditions, the measured voltage and memory voltage are identical. The mho characteristic, a circle in the complex R-X impedance plane, passes through the origin. Once a fault occurs, the measured voltage immediately diverges from the memory voltage, causing the mho circle to expand dynamically.

This dynamic expansion temporarily improves the relay's reach, allowing it to detect faults more dependably under transient conditions. As time progresses, the memory voltage decays using post-fault measured voltages. Consequently, the previously expanded mho circle shrinks, eventually returning closer to its original steady-state shape once the memorized and measured voltages again become equal.

Fig. 8 illustrates the dynamic behavior of a mho element that uses the positive-sequence memory voltage ($V1_{MEM}$) for polarization. For a forward fault, the expansion typically occurs into the third quadrant of the R-X plane.

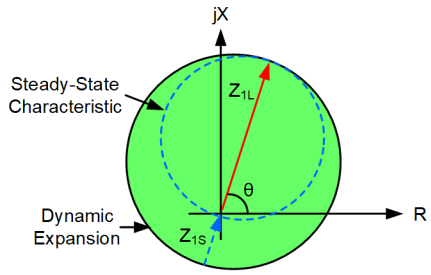

Fig. 8. Dynamic expansion of a mho distance element polarized by positive-sequence voltage in a high-inertia system powered by conventional resources

The effective performance of this dynamic expansion depends on several implicit assumptions in the relay design:

- **Stable Angle Behavior.** The system is assumed to have high-inertia sources, ensuring that the phase angle between the memory voltage and measured voltage remains the same within the relay's operating time.
- **Inductive Source Impedance.** The source impedance behind the relay is assumed to be predominantly inductive, like the line in the forward direction. This helps provide adequate angular separation between forward and reverse fault detection zones.

The use of $V1_{MEM}$ for polarization enhances fault detection sensitivity during transients while retaining directional security, especially for close-in three-phase faults where other polarizing signals are inadequate.

In modern microprocessor-based relays, the directional elements and faulted phase identification logic supervise distance elements to improve their overall reliability.

IV. Transmission Line Protection Challenges

This section presents a series of short-circuit events that illustrate the non-universal and non-deterministic current behavior of IBRs, a stark contrast to the consistent and predictable short-circuit response of conventional synchronous generators. These events not only highlight the waveform anomalies introduced by IBRs but also demonstrate the

responses of protective relay elements to these atypical signals, emphasizing the growing challenges in ensuring reliable transmission line protection.

This section is divided into five subsections. The first two sections present short-circuit events involving partial and full converter-interfaced IBRs. In these events, the IBRs' controlled short-circuit current responses introduce unreliable directional element decisions, misidentification of faulted phases during ground faults, and unpredictable dynamic expansion of memory-polarized distance element characteristics. The third subsection focuses on the high rate of decline of frequency after a short circuit that degraded distance relay performance. The fourth subsection presents two external faults that caused the relay to declare a loss-of-potential (LOP) condition, disabling the supervised directional and distance elements. The last subsection outlines the risks of automatic reclosing on the tie lines interconnecting IBR facilities.

A. Short-Circuit Faults: Partial Converter-Interfaced IBR

In this subsection, three events from three different Type III wind generation facilities illustrate transmission line protection challenges.

1) Evolving Ground Fault—August 2014

Fig. 9 illustrates a 230 kV radial transmission system integrating two Type III WTGs rated at 170 MW and 140 MW, respectively, into the utility grid. An evolving fault occurred on the transmission line connecting the grid to the 170 MW wind generation facility. The fault was initially a Phase-B-to-ground short circuit and, after approximately three cycles, the arc extended to include Phase C, evolving into a phase-to-phase-to-ground short circuit.

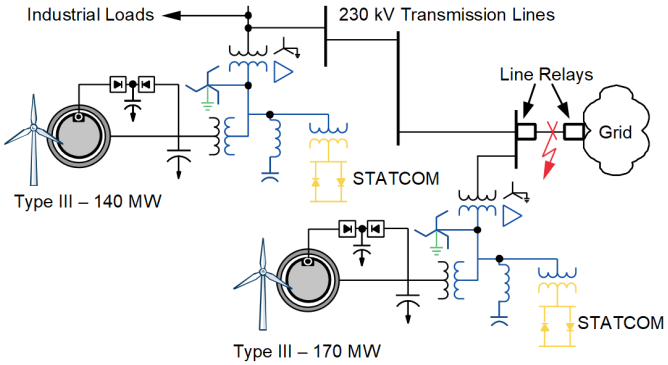

Fig. 9. A 230 kV radial transmission network integrating two Type III wind generation facilities

Fig. 10 presents the data captured by the line protective relays installed at both the grid and WTG terminals. The waveforms were preprocessed by a 60 Hz bandpass digital filter. Line protection uses distance elements supervised by 32Q elements at both terminals. The figure also includes phasor diagrams depicting the angular relationships between the sequence components of the line voltages and currents at approximately 48 ms on the time scale (orange time cursor), corresponding to the Phase-B-to-ground fault and shortly before it evolved to a Phase-B-to-C-to-ground fault.

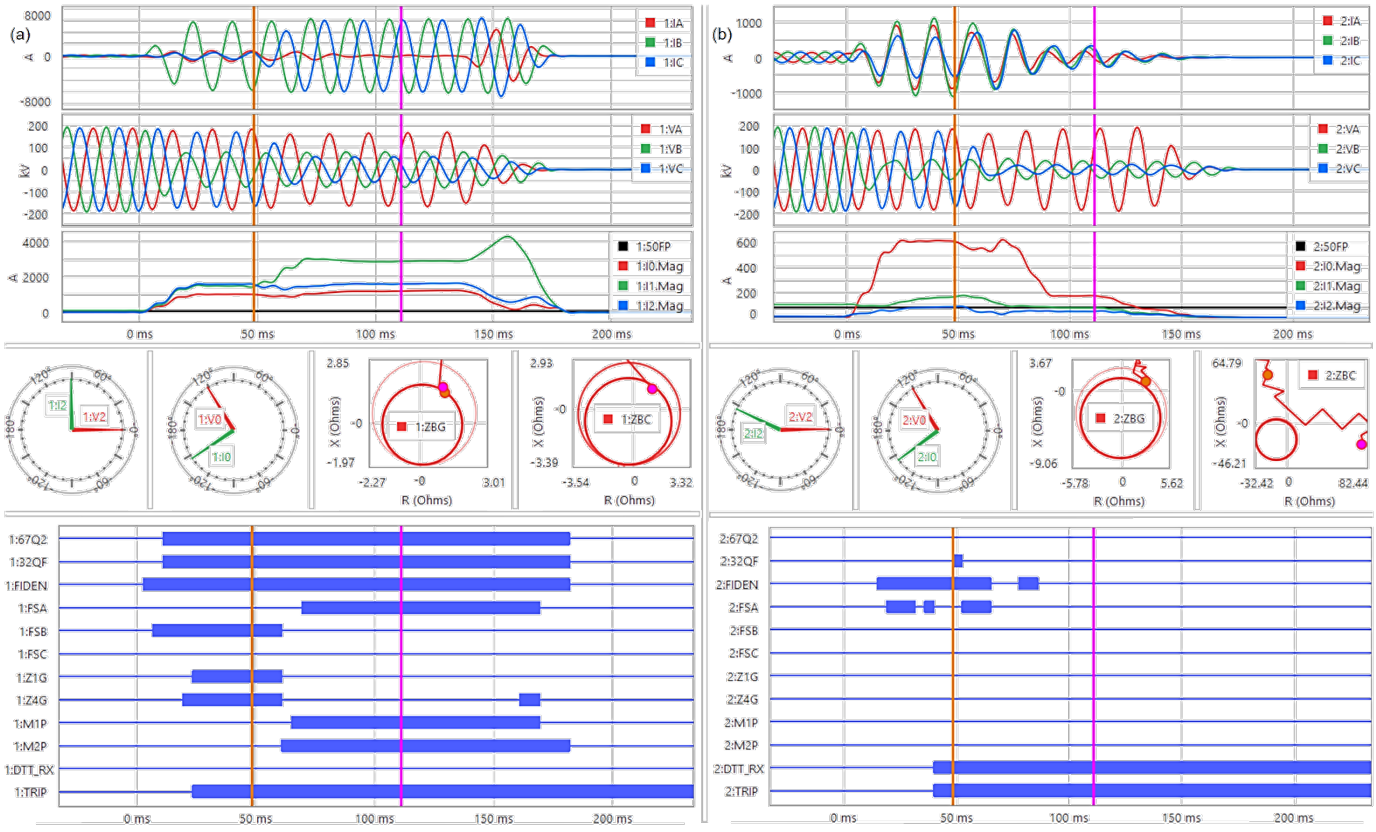

Fig. 10. Evolving BG to BCG fault records from line relays at the a) grid terminal and b) Type III wind generation terminal

a) Relay Responses

At the grid terminal, the I_2 from the grid led the bus voltage by approximately 90 degrees, and the relay correctly identified the forward fault. Though not explicitly shown, the two phasor diagrams indicate that the I_2 lagged I_0 by approximately 120 degrees correctly identifying the Phase-B-to-ground fault before it evolved to a multiphase fault. Because the fault was close to the grid terminal, the Zone 1 ground distance (Z1G) element at that terminal operated within one cycle. When the arc subsequently extended to Phase C, the related phase mho Zone 1 (M1P) and Zone 2 (M2P) elements also responded. The Zone 1 ground distance element issued a direct transfer trip (DTT) to the remote terminal. In addition to the distance elements, the protection scheme included a directional negative-sequence overcurrent (67Q2) element supervised by the 32Q element. The 32Q and 67Q2 elements asserted within one cycle of fault inception.

At the wind generation terminal, the phase distance element did not operate at all, even though the measured impedance entered the ground mho characteristic. This is because the supervising directional element failed to assert. In addition, the relay misidentified the fault as a Phase-A-to-ground fault (FSA asserted) instead of a Phase-B-to-ground fault (FSB did not assert). The terminal eventually tripped after receiving the DTT from the grid terminal.

The phasor diagrams in Fig. 11 are reconstructed using the bus voltages and the current injected by wind generation facilities into that bus. These diagrams provide insight into the partial converter's fault current response.

Before the fault, I_1 lagged the positive-sequence voltage (V_1) by approximately 98 degrees, indicating that the wind generation facilities were supplying predominantly reactive power, while local loads consumed active power. The grid supplemented the active power demand. During the Phase-B-to-ground fault, I_1 magnitude increased from approximately 100 A to 170 A, and its phase angle shifted slightly to about 93 degrees, mimicking a synchronous machine's angular response under fault conditions. However, the I_1 magnitude was significantly lower than that anticipated from a synchronous generation facility with a similar rating.

The I_2, negligible before the fault, increased to about 90 A. Though it was also significantly less than what is anticipated from the synchronous facility, it was consistently higher than the relay's directionality threshold (50FP). Yet, 32QF only asserted transiently for this forward fault. This is because I_2 led V_2 by 155 degrees, diverging significantly from the 90 degrees lead typical of synchronous machines. This phase angle deviation prevented the 32Q element from being dependable for the forward fault. Further, the phase angle of I_2 lagged I_0 by less than 60 degrees and was within the FSA threshold illustrated by the red-shaded region (±60 degrees) in Fig. 6. This caused the relay to incorrectly identify the fault as Phase-A-to-ground.

Note that the angular relationship of I_2 from the Type III wind generator—relative to V_2 or even I_0—remained fairly stable on the wind generator side throughout the fault duration. This angular consistency suggests that the Type III wind generators, with an asynchronous generator and partial converter interface, might maintain a relatively fixed phase relationship during a disturbance.

The phasor diagram also illustrates the I_0 behavior; its magnitude increased significantly, and it led V_0 by approximately 90 degrees. This response was like the one observed by the grid relay. The consistency in zero-sequence behavior stems from the wye-grounded–delta (YNd) transformer configuration commonly used to connect IBRs to the transmission system (with the wye-grounded winding connected to the high-voltage transmission network). This winding configuration presents an effective zero-sequence path during ground faults, independent of the type of generation connected downstream of the transformer.

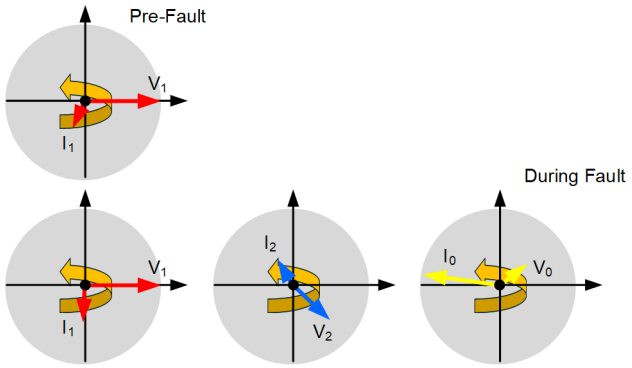

Fig. 11. Phasor diagrams based on data captured by the line protection system at the wind generation terminal during the BG fault

2) Remote Ground Fault—August 2020

Fig. 12 depicts a 132 kV radial transmission system integrating a Type III wind facility composed of 55 units, each rated at 1.8 MW. In this installation, the line protection utilizes distance elements supervised by the 32V element. During this event, an external single-line-to-ground fault occurred on the transmission system three lines away. Although the wind generation facility successfully rode through the external fault, the remote protection system issued a DTT signal via the anti-islanding scheme, resulting in the facility's disconnection.

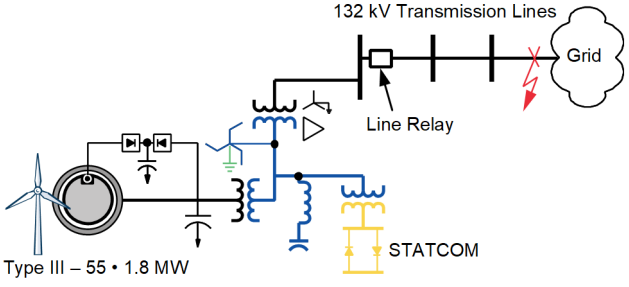

Fig. 12. A 132 kV radial transmission network integrating a Type III wind generation facility

Fig. 13 presents waveforms captured by the line protective relay at the WTG terminal, showing the dynamic response of fault quantities and the associated protection element response.

Prior to the fault, the wind generation facility delivered approximately 34 MW of active power and absorbed about 5 MVAr of reactive power. Upon fault inception, the active power output decreased sharply while the facility attempted to support the voltage dip by injecting reactive power—a typical response of Type III wind turbines during voltage sag conditions.

During the fault, I_1 decreased from 240 A to 158 A, which was exactly the opposite of the anticipated increase in I_1 from synchronous generation. The I_2 increased from near zero to about 180 A—greater than I_1, which is not typical. Note that the phase angle of I_2 led V_2 by approximately 130 degrees, once again significantly greater than the 90 degrees anticipated from synchronous generation.

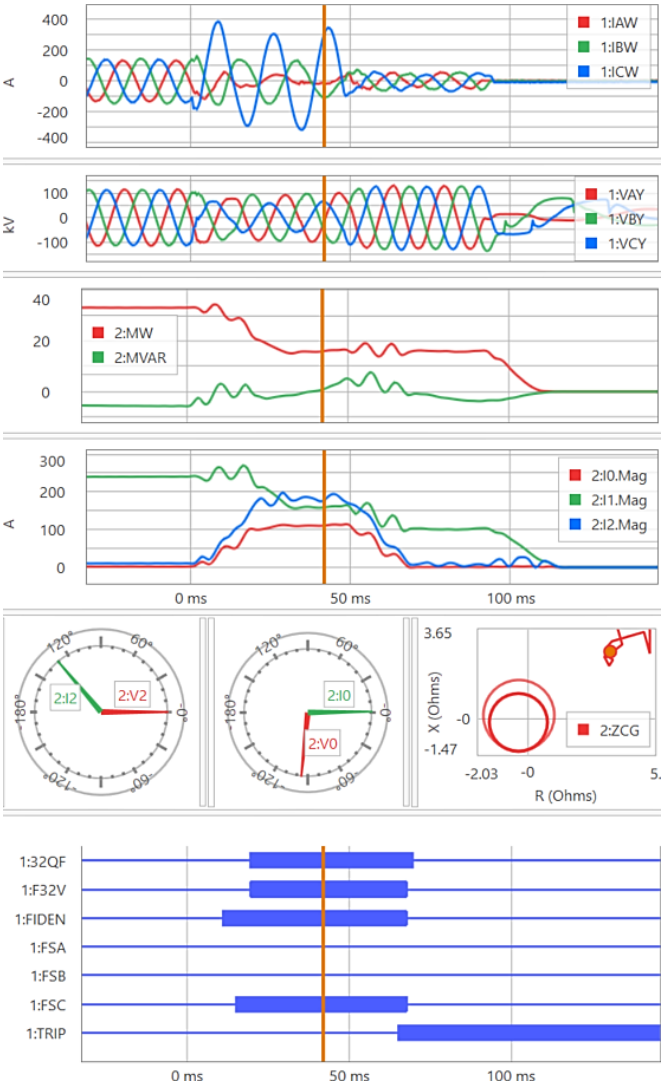

Fig. 13. Line relay recordings from a Type III wind generation facility for an external CG fault

In this application, the 32V element (using zero-sequence measurements) operated correctly, attributed to the zero-sequence path presented by the YNd transformer configuration. It declared a forward fault because I_0 led V_0 by about 90 degrees. Furthermore, the phase angle between I_2 and I_0 remained stable throughout the duration of the fault. With I_2 leading I_0 by approximately 120 degrees, the faulted phase identification logic firmly asserted FSC, indicating a Phase-C-to-ground fault.

Fig. 13 further illustrates the behavior of the ground mho element under these conditions. The mho characteristic exhibited a dynamic expansion in the reverse direction, based on $V1_{MEM}$ polarization, a response similar to what we anticipate from synchronous generators. This observation suggests that the ground distance element would have operated correctly if the fault was within the protection zone.

3) Phase-to-Phase Fault—March 2022

Fig. 14 depicts a 78-mile 230 kV line interconnecting an aggregated 575 MW of Type III WTGs. There are capacitor banks with an aggregate 200 MVAr rating 0.5 miles away from the grid terminal. The line relays in this installation utilize phase and ground Zone 1 and Zone 2 mho elements set to approximately 85 percent and 125 percent of the line impedance, respectively. The IBR relay Zone 1 is set to trip instantaneously and Zone 2 is set to trip with a 30-cycle delay. The grid relay Zone 1 is set to trip with a 6-cycle delay to allow the capacitor bank protection to clear faults first and Zone 2 is set to trip with a 20-cycle delay. Current differential protection using a three-terminal scheme is also applied.

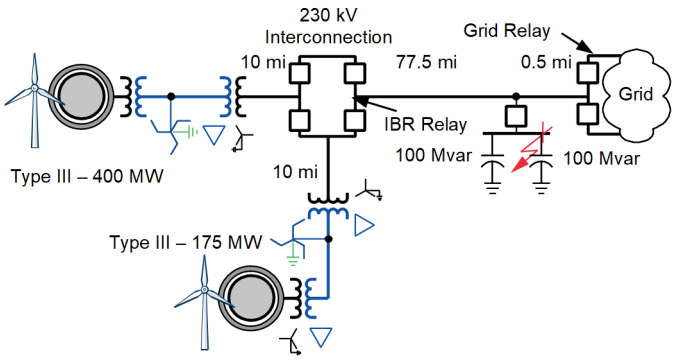

Fig. 14. A 230 kV line interconnecting 575 MW Type III wind generation

There was a Phase-C-to-A fault beside one of the capacitor banks near the grid terminal. Fig. 15 shows the unfiltered phase currents and voltages from the IBR and grid relays. When the fault occurred, about 400 MW of generation was on.

The 32Q element and faulted phase identification logic in the IBR relay behaved well and were consistent with the grid relay. The fault was detected in the forward direction. I_2 led V_2 by approximately 130 degrees, like the previous event in Section A.2. The faulted phase identification outputs, FSA, FSB, and FSC, correctly did not assert in the absence of I_0, allowing the phase distance (ZCA) element to be dependable.

The Zone 1 phase mho (M1P) element at the grid terminal operated dependably for the close-in fault, 0.5 miles away. It started timing (with a 6-cycle delay), allowing the capacitor bank protection sufficient time to trip and clear the fault. On the other hand, at the IBR terminal, M1P transiently overreached two cycles after fault inception, causing the IBR terminal to trip and lose 400 MW of generation.

The M1P overreach was for a fault beyond 99 percent of the line impedance when its reach was set to 85 percent, a significant overreach. Transient overreaches are sometimes associated with voltage measurement errors due to a high source-to-line impedance ratio (SIR). However, during this event, the Phase A voltage at the IBR terminal did not collapse as much as that of Phase C. At the time of M1P overreach, the CA loop voltage was 35 percent of the nominal. In fact, the unfaulted Phase B voltage was slightly smaller than the faulted Phase A voltage, which translated to a smaller unfaulted BC loop voltage than the faulted CA loop voltage. The voltage magnitudes decayed during the fault.

Referring to the fault loop apparent impedance (ZCA), we notice significant oscillations. Additionally, the large angular difference between $V1_{MEM}$ and V1 caused an expansion and shift of the mho characteristics toward the second quadrant. These two behaviors caused M1P to overreach transiently. In contrast, the grid relay calculated a stable ZCA. Its mho expansion was toward the third quadrant, as is typical in an inductive system with synchronous generators.

We conclude that the control response of IBRs during phase faults (without ground involvement) can cause phase distance elements to exhibit significant transient overreach. The fault voltages may also exhibit unusual behavior—the unfaulted phase (and loop) voltages may be lower than the faulted phase (and loop) voltage.

4) Protection Impairments and Observations

The following protection impairments and key observations are derived from the three short-circuit events (Sections A.1 through A.3) recorded at three different Type III WTG facilities:

- **I_2 Behavior:** Type III WTGs can contribute some level of I_2 in response to unbalanced terminal V_2. The phase angle of I_2 was stable relative to V_2 but significantly exceeded 90 degrees.
  - In one event, I_2 led V_2 by 155 degrees, reducing 32Q element dependability and causing incorrect faulted phase identification.
  - In two other events, I_2 led V_2 by 130 degrees, providing correct directionality and faulted phase identification.

Recent literature [9] highlights the inherent limitations of I_2 injection from these turbines. The variability observed from the events suggests dependence on converter control behavior. It is worth noting that the high angle lead of I_2 with respect to V_2 (compared to synchronous generation) challenged directional element dependability but did not cause a loss of security. Quadrilateral elements polarized by I_2 are also expected to incur significant reliability risks.

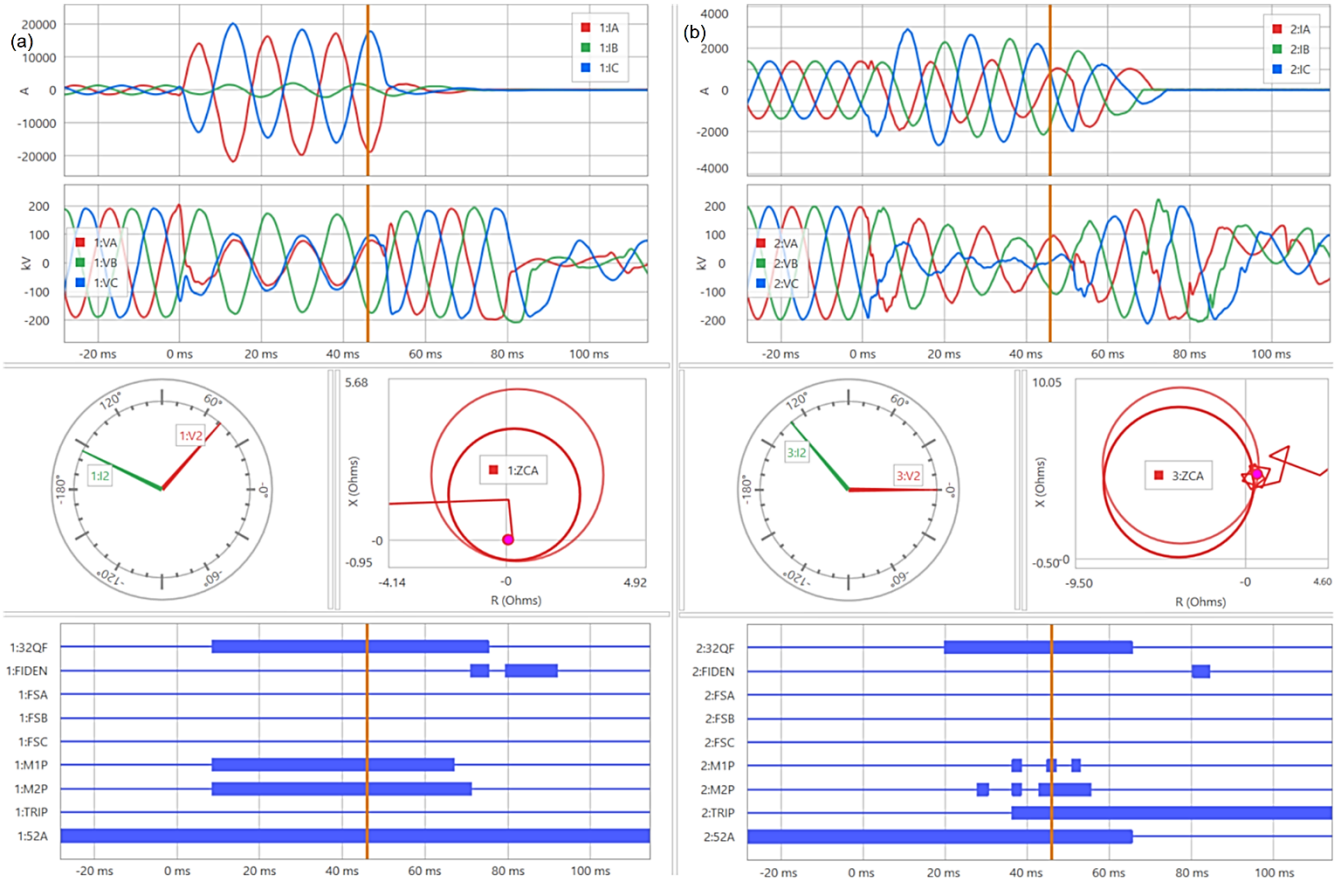

Fig. 15. Phase-C-to-A fault records from line relays: a) grid relay and b) IBR relay

- **Voltage Behavior:** Although not used by the relays, the voltages at the IBR line terminal provided a reliable indication of ground fault type (e.g., Fig. 7). However, using just voltages may not be sufficient for phase-to-phase faults.
- **Unpredictable Transient Response of the Phase Mho Element:** The dynamic expansion of the phase mho element at the IBR terminal was found to be unpredictable, primarily due to significant phase shift between the pre-fault (memory) and the fault voltages. This contributes to Zone 1 transient overreach impacting security. The apparent impedance also exhibited significant transient oscillations, which contributed to reduced Zone 2 dependability.
- **Zero-Sequence Directional Element Reliability:** Zero-sequence directional elements perform reliably when the IBR is connected through a transformer with a winding that presents a path for I_0.

These observations illustrate that Type III WTG control strategies can compromise the effectiveness of traditional protection schemes. Tailored relay settings, enhanced logic supervision, and control-aware protection designs are needed to ensure reliable performance.

B. Short-Circuit Faults: Full Converter-Interfaced IBR

This subsection presents four faults from solar generation facilities, demonstrating that the I_2 supplied by the inverter drifted out of sync with the system voltage, leading to three misoperations of protection elements on reverse faults and one faulted phase misidentification.

1) Reverse Ground Fault Seen as Forward—June 2021

As shown in Fig. 16, a 160 MW solar generation facility is connected to a utility transmission station via a 345 kV tie line.

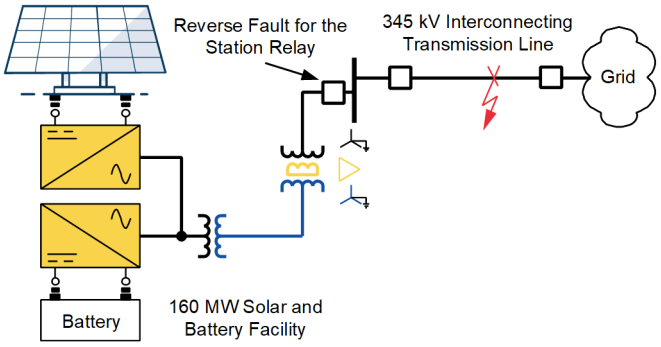

Fig. 16. 345 kV transmission line integrating 160 MW solar and battery generation to the utility grid

A Phase-A-to-ground fault occurred on the interconnecting transmission line. From the perspective of the station protective relay, which looked toward the IBR, this was a reverse fault. Fig. 17 shows the waveforms captured by this relay, detailing both the fault signatures and the behavior of protection elements.

The fault current during the event was dominated by I_0, primarily available due to the delta-tertiary winding of the interconnecting transformer. The relay was configured with 32Q elements, which toggled from reverse to forward declaration during the event. This toggling behavior can be explained by examining the angular relationship between I_2 and V_2 during the fault.

Phasor diagrams captured at the 30 ms time stamp show that I_2 leads V_2 by 110 degrees, which the relay logic typically interprets as a forward fault (in a system with synchronous generators). However, in this case, the fault was actually in the reverse direction.

The root cause of this angular variation lies in the grid-following behavior of the inverter. While the system voltage—and therefore the V_2 phasor—remained relatively stable due to the grid's strong inertia, the inverter's output current did not maintain a stable frequency. Because the inverter lacked significant inertia, it exhibited transient oscillations under fault conditions, causing the I_2 phasor to drift relative to the voltage phasor, leading to directional misinterpretation.

Further examination of the phasor diagram shows that I_2 led V_2 by 110 degrees, incorrectly suggesting a forward fault. I_0 lagged V_0 by 90 degrees, correctly indicating a reverse fault because of the zero-sequence path presented by the YNynd transformer.

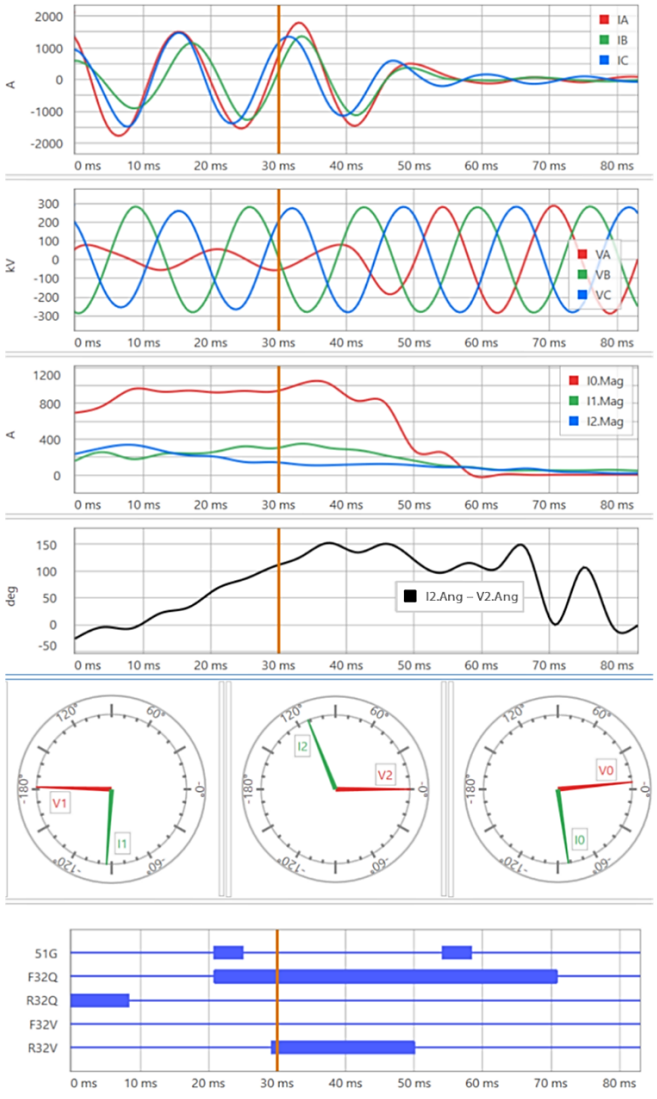

Fig. 17. Relay records from the station line protective relay for the reverse Phase-A-to-ground fault

2) Reverse Ground Fault Seen as Forward —January 2024

This event involves misoperation of the line protective relays, supplied by two IBR facilities, for a reverse fault. Fig. 18 shows two solar generation facilities, connected through a 230 kV four-breaker ring bus switching station (Station C), segmenting an existing transmission line between two grid terminal stations, A and B.

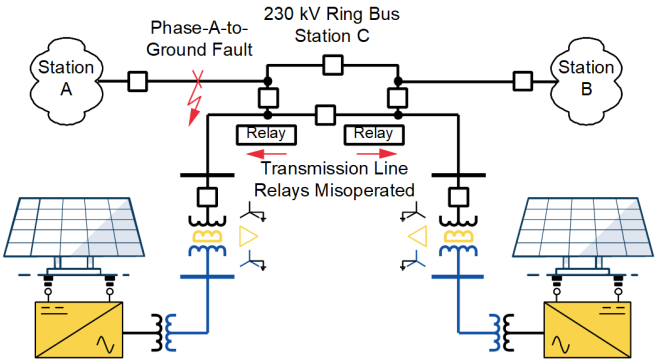

Fig. 18. A 230 kV ring bus switching station integrating two solar generation plants into the utility grid

A Phase-A-to-ground fault occurred on the 230 kV transmission segment between Stations A and C, near Station C. The line protective relays at the transmission line terminals (Stations A and C) operated correctly to isolate the fault. However, the protective relays on the two interconnection lines to the solar IBRs misoperated.

Fig. 19 shows the record captured by one of the line protective relays that misoperated. The sequence of events was as follows:

- The solar facilities were exporting approximately 35 MW at the time of the event.
- A Phase-A-to-ground fault occurred on the Station A–Station C 230 kV line, near Station C.
- The IBRs contributed fault current for approximately 3 cycles.
- The line protection on the Station C–Station A line operated correctly.
- The protective relays on both interconnection lines to the IBRs misinterpreted the fault as being in the forward direction.

The incorrect operation of the interconnection line protective relays led to the tripping of all four ring-bus breakers at Station C, which activated the anti-islanding scheme.

These two misoperating elements were 67Q elements that were supervised by 32Q elements and configured to detect forward faults looking into the solar generation facilities. Due to the limited and controlled fault contribution from the IBRs, the 32Q elements on these relays interpreted the IBR-supplied fault current as being in the forward direction, despite the actual fault being external and in the reverse direction relative to the relays' line terminals.

In contrast, the protective relays on the faulted transmission line correctly identified the fault direction due to stronger I_2 flowing from the grid sources at Stations A and B. However, the IBR relays' misinterpretation triggered the operation of the interconnection line protective relays, which led to the tripping of both interconnection lines.

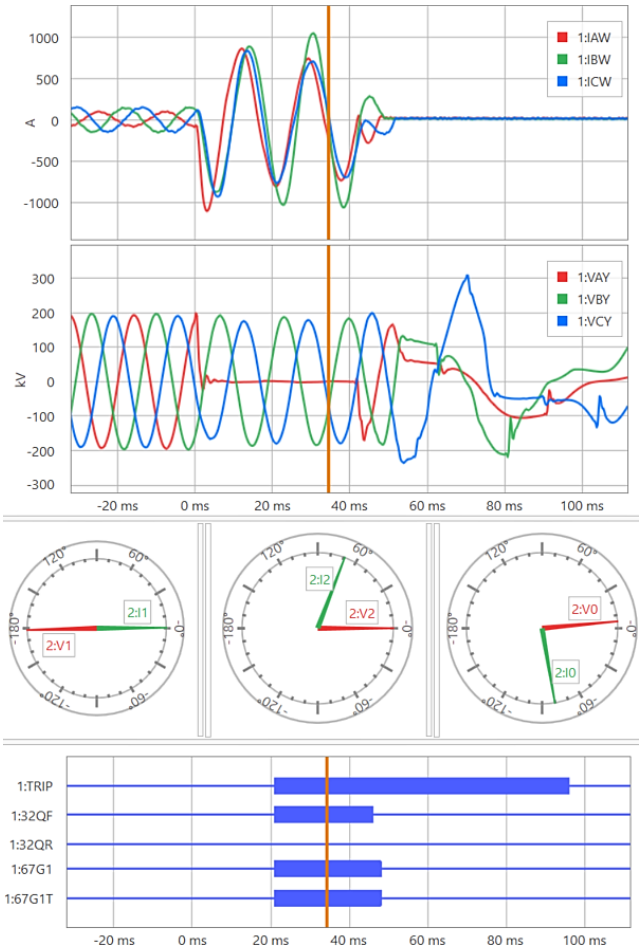

Fig. 19. The fault record captured by one of the station relays misoperating on the reverse fault

3) Misidentified Phase on a Ground Fault—March 2021

Fig. 20 is a one-line diagram showing a 145 MW Type IV wind generation facility connected to the utility transmission system through a 230 kV line.

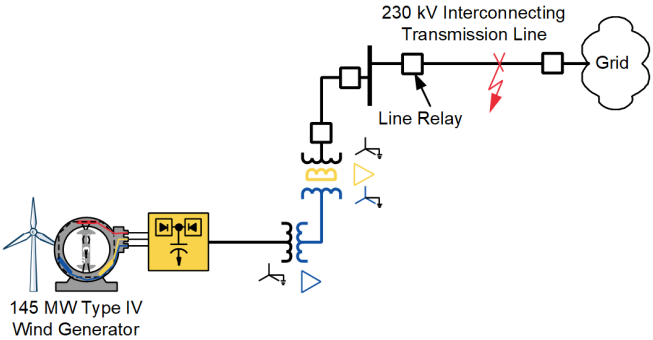

Fig. 20. Integration of 145 MW Type IV wind generation into the 230 kV transmission system

A phase-to-ground fault occurred on the transmission line connecting the wind facility to the grid. Fig. 21 shows the bus voltages and fault current recorded by the transmission line protective relay facing toward the fault. The complete collapse of Phase A voltage unambiguously indicates a Phase-A-to-ground fault.

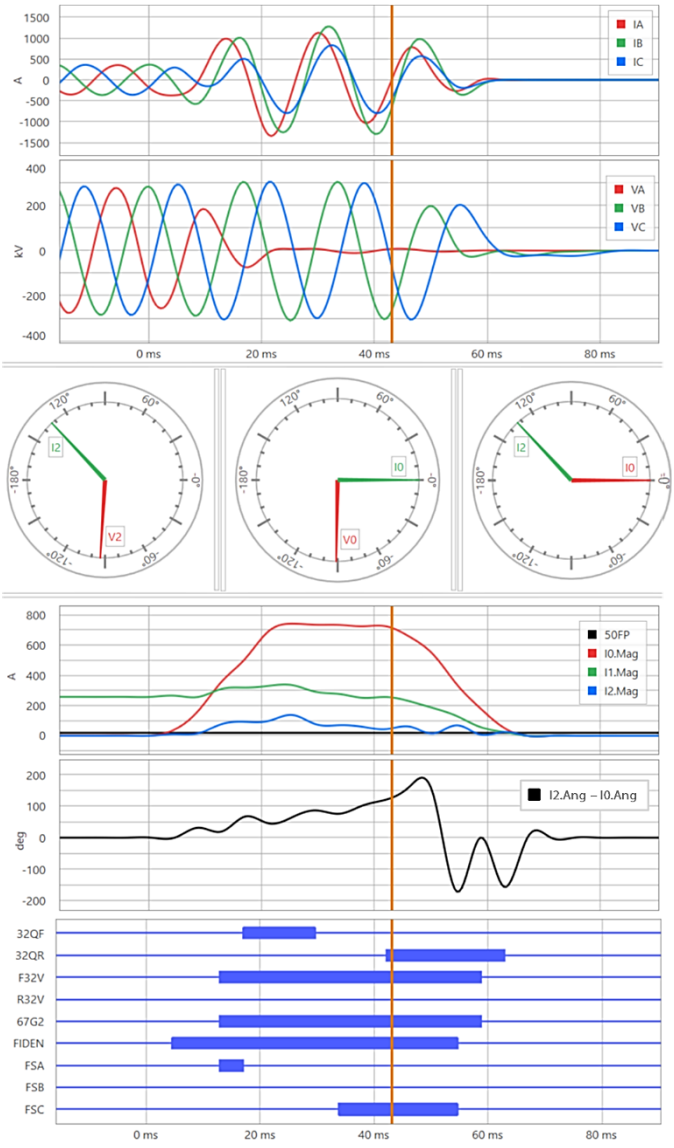

Fig. 21. Type IV wind generator response during a Phase-A-to-ground fault

In Fig. 21, the I2.Ang – I0.Ang plot illustrates the angular difference between I_2 and I_0, which was continuously varying while the fault persisted. The key observations are:

- I_2 is supplied primarily by the IBR and exhibits frequency instability due to the lack of inertia in grid-following mode.
- I_0 is largely available due to the transformer's delta tertiary winding and remains at a stable 60 Hz.

Due to the mismatch in the frequencies, the relative phase angle between I_2 and I_0 rotated unpredictably. As a result, the faulted phase identification logic based on the relative angle relationship between I_2 and I_0 misclassified the faulted phase as Phase C, even though the actual fault occurred on Phase A.

4) *Permissive Trip on an External Ground Fault—March 2022*

This event originated near a 30 MW solar facility, shown in Fig. 22. A line protective relay responding to the ground fault current contribution from this facility transiently asserted forward on a reverse fault and issued a permissive trip signal, causing a misoperation.

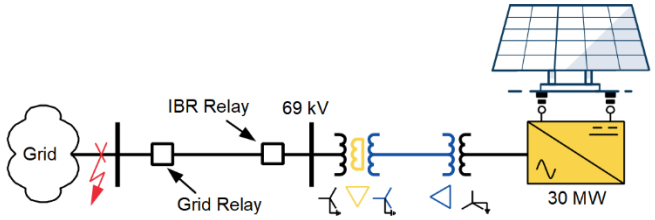

Fig. 22. External ground fault near a 30 MW solar facility

Fig. 23 presents the relay records from both terminals of the transmission line. A Phase-A-to-ground fault was located behind the grid-side relay (reverse direction) and in front of the IBR-side relay (forward direction). The faulted phase voltages at the IBR terminal remained elevated, indicating that the fault was electrically remote from the solar facility.

Both line protective relays employed forward-looking ground directional overcurrent (67G2) elements that were controlled solely by the 32Q element. The 67G2 element at the grid terminal misoperated. The sequence of events is summarized as follows:

- t = 0 ms: A Phase-A-to-ground fault occurred on the line.
- t = 22 ms: The grid-side relay incorrectly asserted a forward-directional fault via 67G2 for half a cycle and keyed a spurious permissive trip (PT) signal to the IBR-side relay.
- t = 42 ms: The IBR-side relay receives the permissive trip signal. It has already correctly detected a forward fault using 67G2. Therefore, it initiates a trip.

Both relays see the same current (ignoring polarity) and similar voltages (very short line). Because I_2 keeps rotating with respect to V_2, the fault initially appears to be toward the IBR. The grid relay declares a forward fault incorrectly and sends a permissive signal to the IBR relay. I_2 continues to rotate with respect to V_2 and by the time the permissive signal arrives at the IBR relay, the fault appears to be toward the grid (correctly). The changing nature of the I_2 contribution from the IBR, in conjunction with the channel delay, caused the misoperation. Because external ground faults are quite common, this event illustrates one of the most common types of line relay misoperations near IBRs.

Another observation from this event is that the fault current contribution from the IBR is quite small. Removing I_0 from the phase currents, the IBR phase currents were about one-third of the pre-fault load current.

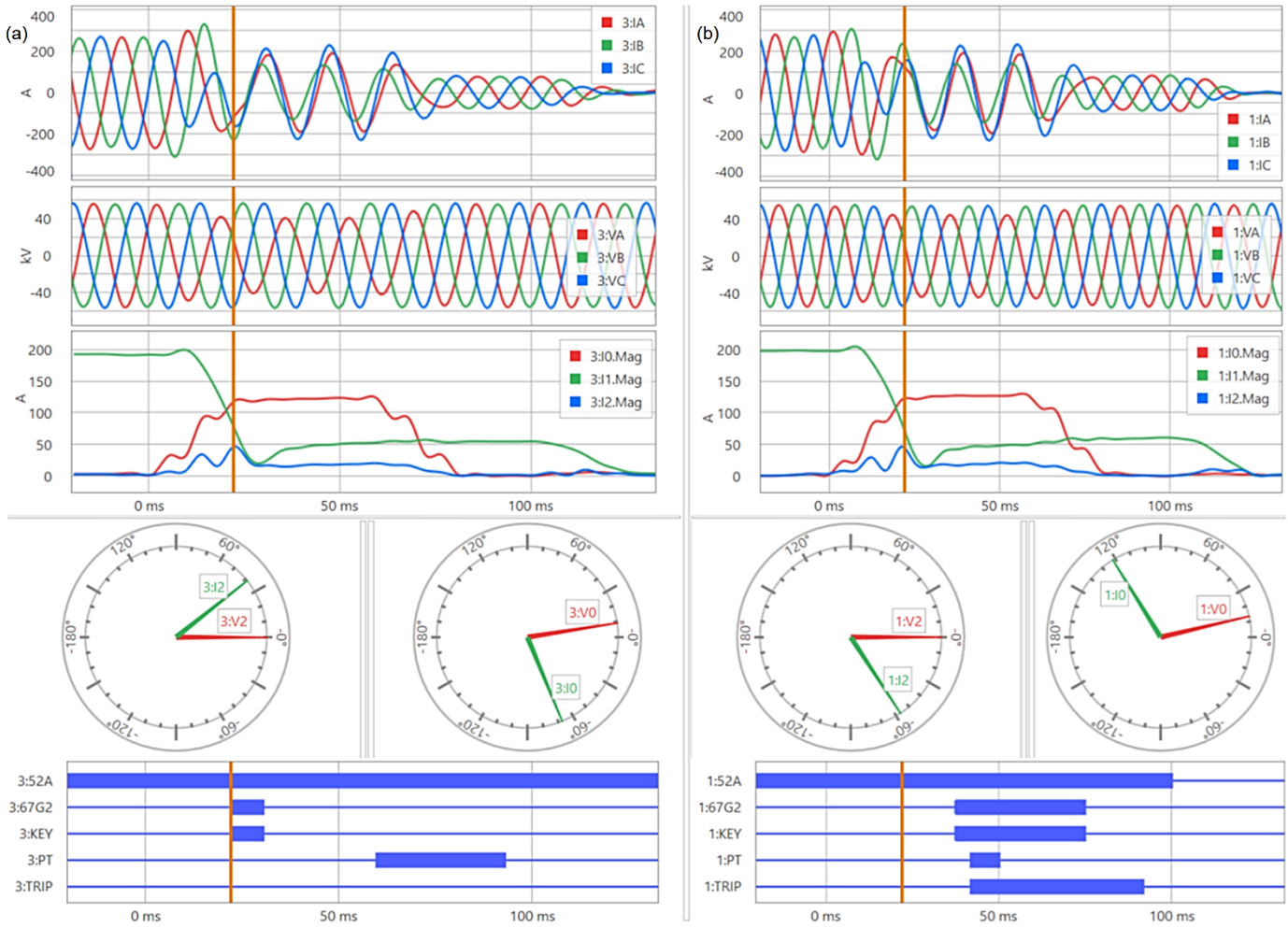

Fig. 23. Misoperation of a permissive scheme for an external ground fault as shown by a) the grid relay and b) the IBR relay

5) Protection Impairments and Observations

Solar facilities are full converter-interfaced IBRs, similar in behavior to a Type IV wind generator, and operate in a grid-following mode, synchronizing their output to the grid voltage. A common misconception is that a grid-following inverter remains phase-locked to the grid as long as it is energized. However, the presented events revealed that during fault conditions, the inverter contributed minimal I_2 and lost synchronization with the system voltage. This behavior impairs line protection performance due to the following key issues:

- **Directional Element Performance:** The 32Q element can lose both security and dependability in systems with full converter-interfaced IBRs. This is unlike partial converter-interfaced IBR systems (Type III) where there was only a loss of dependability.
- **Faulted Phase Identification:** The non-deterministic phase angle relationships between I_2 and I_0 can cause a misidentification of the faulted phase, just like in systems with partial converter-interfaced IBRs.

Zero-sequence protection remains immune from converter control as long as the IBR is connected to the transmission through a transformer that presents a path for I_0.

C. Fast Frequency Excursion During Evolving Phase Fault—October 2023

This event originated at a Type III WTG facility. During an evolving phase fault that remained uncleared for half a second, the WTG exhibited a rapid rate-of-change of frequency (ROCOF), which adversely affected the relay's frequency tracking algorithm and degraded the performance of memory-polarized distance protection.

There were 24 MW of Type III WTG in a 50 Hz system that was connected via a 15.7 km 66 kV line, as shown in Fig. 24. The line was protected by three phase mho and three ground quadrilateral step-distance zones. Zone 1 was set to trip instantaneously, and Zones 2 and 3 were set to trip with a 20-cycle (0.4 s) and 50-cycle (1 s) delay, respectively. Fig. 25 shows the response captured by the wind facility relay for the evolving phase fault. The sequence of events is as follows:

- A Phase-A-to-B fault occurred. The fault was external to the protected line and outside Zone 3.
- After 62 ms, the fault arc extended to include Phase C and evolved to a three-phase fault, remaining uncleared for some time.
- At 436 ms, the Zone 1 phase mho element on the CA phase loop misoperated. 50 ms later, the fault was cleared from the WTG terminal.

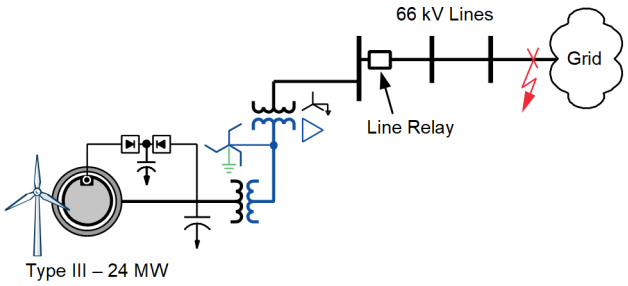

Fig. 24. Remote external phase fault in a Type III wind generation system

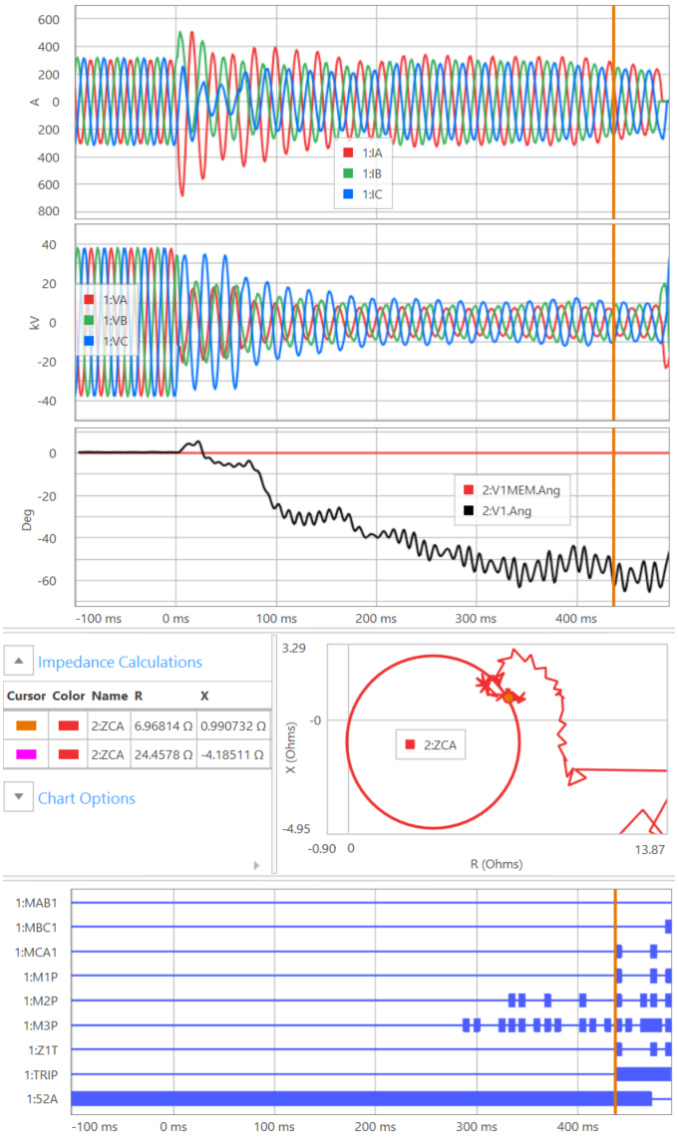

Fig. 25. Type III wind generation response for an external evolving phase fault

The fault was uncleared for a significant duration, which caused corruption of the positive-sequence memory voltage used by the distance relay. Initially, the phase angles of the real-time V_1 and memory V_1 ($V1_{MEM}$) were aligned. However, immediately after fault inception, the two began to diverge (V_1 slowed down), reaching a 60-degree phase angle difference at 436 ms when Zone 1 misoperated. This divergence significantly impacted the relay's operation:

- The dynamic expansion of the mho characteristic deviated significantly from what is expected (see Section III.C), shifting from the third quadrant to the fourth quadrant on the R-X plane.
- As a result, Zone 1 phase distance element ZCA picked up incorrectly and tripped erroneously, despite the fault being external.

To investigate further, the waveform data were exported to MATLAB, and the frequency was calculated using zero-crossing analysis of the voltage waveform. The alpha voltage ($V\alpha = VA - 0.5 \cdot VB - 0.5 \cdot VC$) was used to remove any common-mode zero components in the voltages. The alpha voltage and its corresponding frequency are shown in Fig. 26. During the fault, the system frequency dropped from 50 Hz to below 42.5 Hz, a deviation greater than 7.5 Hz. The ROCOF exceeded 25 Hz/s during the marked interval. Notably, this occurred even though the WTG was online, although there was a three-phase fault between the WTG and the grid. This event demonstrates how IBRs can induce fast frequency decline, impairing memory-polarized distance relays.

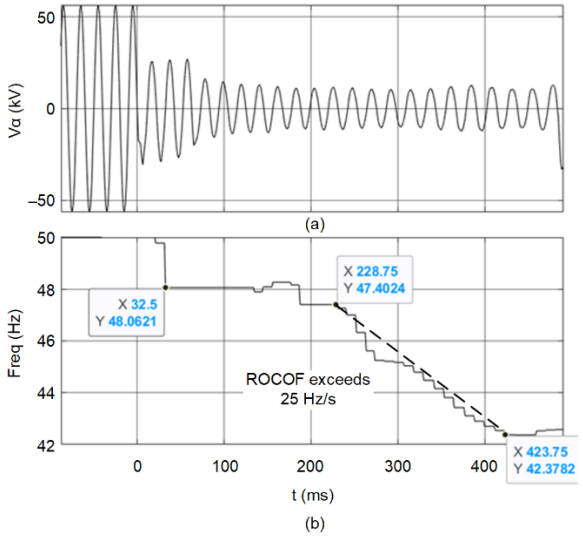

Fig. 26. a) Alpha voltage and b) frequency calculated using its zero-crossings

D. *Loss of Potential Risking Protection Dependability*

The loss of potential (LOP) detection logic used in most protective relays is traditionally based on the behavior of synchronous generators, which exhibit a high-magnitude fault current concurrent with voltage depression during short-circuit conditions. However, this assumption does not hold for IBRs. This subsection presents two external three-phase short-circuit events that highlight how the controlled short-circuit current response from IBRs can mislead the protection system into falsely declaring an LOP condition, thereby impairing protection reliability.

1) *External Three-Phase Fault—May 2024*

Fig. 27 shows an external three-phase fault that occurred on a remote 230 kV transmission line interconnecting two solar generation facilities totaling 225 MW. These facilities, based on full-converter inverters, were integrated into the utility transmission grid via step-up transformers.

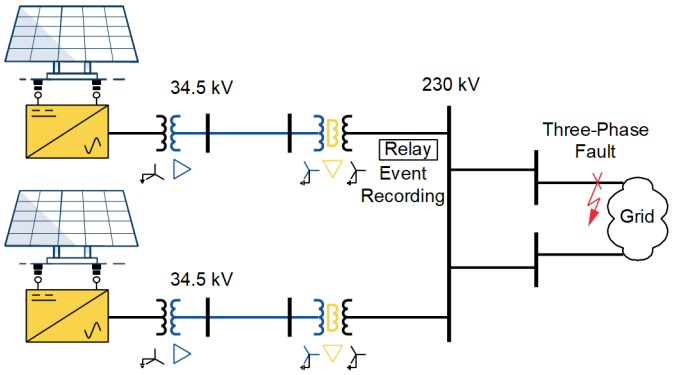

Fig. 27. 225 MW solar facility interconnected to the 230 kV system

Fig. 28 presents the oscillography recorded by the 230 kV line protective relay located at the interconnecting substation. This relay was monitoring the line connecting one of the solar facilities and was triggered by the external three-phase fault. The primary protection cleared the fault approximately 100 ms after inception. The following key data were observed:

- Pre-fault voltage: ~102% of nominal
- Fault voltage: ~79% of nominal
- Pre-fault current: ~2.5% of nominal
- Fault current: ~7% of nominal

While the voltage dropped during the fault as expected, the increase in the current was minimal, less than 5 percent of nominal, due to the limited short-circuit contribution from the IBR. This discrepancy between voltage drop and lack of current increase triggered the relay's LOP logic.

Even after the fault was cleared and voltages recovered above 85 percent of nominal, the LOP condition remained asserted for 500 ms. The LOP signal falsely stayed latched even though system conditions had returned to normal, undermining dependability of the voltage-dependent elements (e.g., distance, directional overcurrent, and undervoltage elements).

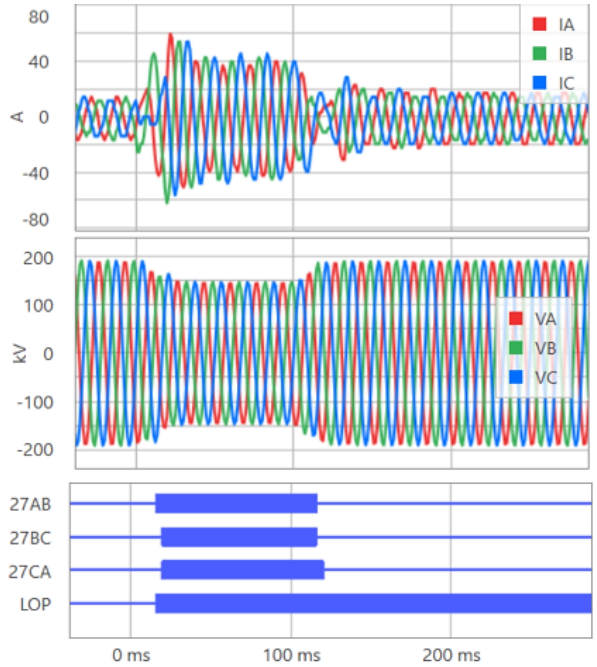

Fig. 28. Extended LOP assertion during an external three-phase fault due to low fault currents

2) External Three-Phase Fault—July 2018

In addition to their inherently low fault current contribution, IBR control behavior during disturbances can further challenge the relay LOP logic.

A Type IV WTG facility is connected to the utility with a 7.5 km long 138 kV line. Significant lightning activity in the area caused an external three-phase fault at a location similar to the one shown in Fig. 27. The fault was cleared by primary protection within approximately 3.5 cycles. Fig. 29 presents the bandpass-filtered oscillography.

During the fault, the IBR maintained a nearly constant output current, despite a significant voltage depression at the terminals. This lack of appreciable current change, combined with the sharp voltage drop, caused the relay's LOP element to assert.

Before the fault was cleared, the IBR entered a momentary current cessation mode, suspending its output entirely. This behavior, where the inverter inhibits current output under abnormal voltage conditions, is discussed in detail in Section V. Once the fault was cleared and the system voltage recovered, the IBR also resumed its output. The resulting increase in voltage magnitude was sufficient to satisfy the LOP reset criteria, and the relay deasserted the LOP condition.

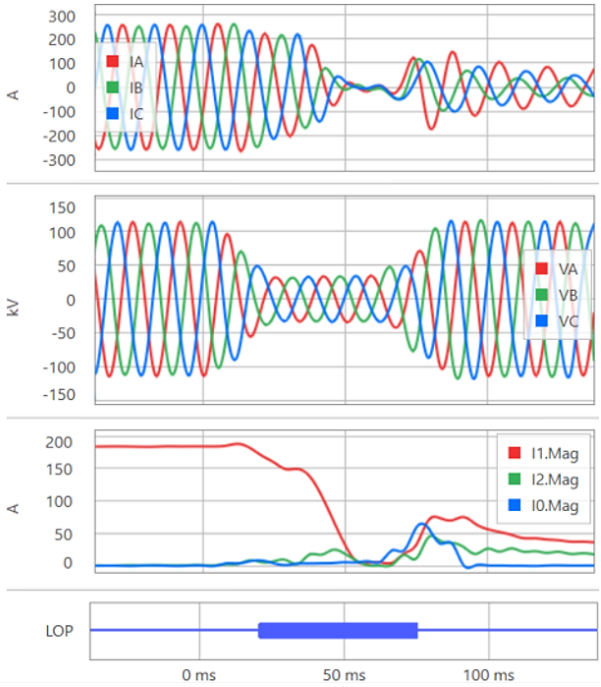

Fig. 29. LOP assertion during an external three-phase fault due to the IBR's controlled response

This sequence illustrates how IBRs can maintain pre-fault current levels during faults, which introduce dynamic changes that standard LOP algorithms are not designed to handle. Because conventional LOP logic relies on measurable changes in magnitude of phase current, I_2, or I_0, external multiphase faults are more likely to result in false LOP assertions, undermining the dependability of phase fault protection. While three-phase fault examples are used in this section, Section V.A includes an event where LOP asserted incorrectly during a phase-to-phase fault.

E. *Reclosing Issues*

Most transmission line faults are single-line-to-ground and transient in nature. They often self-clear once the surrounding air regains its natural dielectric strength following line de-energization [10]. Depending on local atmospheric conditions around the fault, this recovery typically occurs in less than one second. To maintain system stability and minimize outage duration, high-speed automatic reclosing, usually within one second, is widely employed on transmission systems.

When system stability is not a primary concern, a delayed autoreclosing strategy is often adopted. Reclosing times, in this case, typically range from 3 to 20 seconds, allowing additional time for transient fault clearing and reducing the risk of restrikes or asset wear due to repeated reclosing attempts.

For tie lines connecting to generation resources, a pre-check, commonly referred to as a dead-line check, is performed before initiating an autoreclose from the grid side. This check ensures that the line is de-energized and isolated from the generation source, thereby avoiding the risk of out-of-synchronism reclosing. Once the line is successfully re-energized, the generation resource can be properly synchronized and reconnected.

When the faulted line connects to IBRs, additional challenges emerge. After a fault, many IBRs do not immediately shut down but instead enter a temporary suspension or cease mode lasting 10 seconds or longer in some cases, depending on the severity of the disturbance and the inverter's control logic. During this suspension, the inverter ceases current output but may remain electrically connected to the line.

A Phase-C-to-ground fault occurred on a 345 kV line near a Type III WTG facility, shown in Fig. 30. The fault was cleared by the line protective relays in approximately 3 cycles. The unfiltered oscillography of the IBR relay is shown in Fig. 31. The vertical dashed line separates the initial 150 ms following fault inception (left) and the reclosing following 550 ms (right). The voltages are measured on the line side of the WTG facility breaker.

When the breaker closes on the de-energized line, transients in the currents and voltages can be seen, indicating that the WTG facility was still energized.

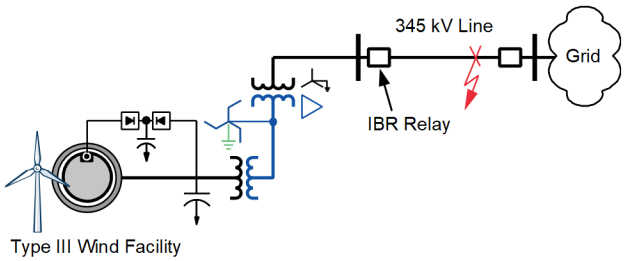

Fig. 30. One-line diagram for a July 2000 Phase-C-to-ground fault

In addition to this event, Section V.A presents a field event where an IBR remained online for 10 seconds following a phase-to-phase fault, during which out-of-synchronism closing was narrowly avoided. Section VI further includes several events showing that IBRs can remain energized for several seconds after they have been disconnected from the grid. The events are all from grid-following IBRs.

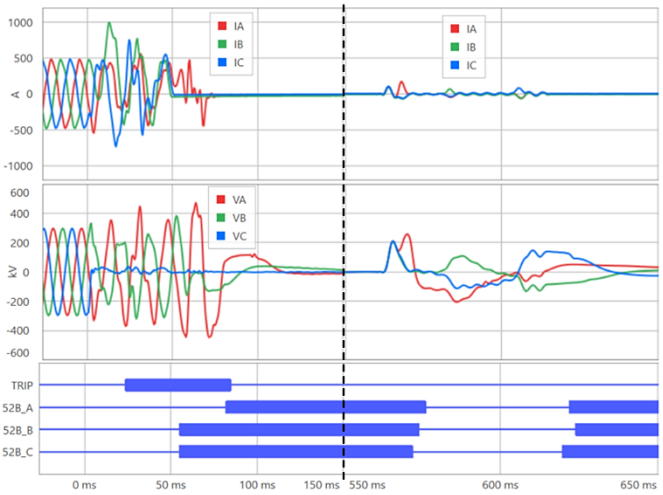

Fig. 31. Reclosing following a Phase-C-to-ground fault in July 2000

When IBRs remain online following a fault, they introduce two significant risks:

1. **Failure to Isolate the IBR:** Because the IBR does not fully disconnect and go offline, the protection system may not detect an islanded condition, allowing an autoreclose to proceed based on a false dead-line condition.
2. **Improper Restart Sequencing:** The IBR may resume operation without completing its required self-diagnostics, such as phase-locked loop (PLL) resynchronization, grid-matching, and start-up logic. This could result in out-of-synchronism closure, posing risks to equipment and system stability.

These challenges highlight the need for carefully coordinated reclosing logic on lines connected to IBRs, including the potential use of:

- Extended dead time settings
- Reclose blocking based on IBR status
- Synchronism-check relays
- Telemetered confirmation of IBR disconnection

V. Cease Mode, Ride-Through, and Reduced Short-Circuit Level

Most grid codes require that IBRs stay online and successfully ride through voltage depressions from external short circuits and disturbances. The events presented in this section illustrate that some IBR designs are riding through these events by suspending their operations and blocking their output currents upon detection of voltage depression. This mode of operation is referred to as the IBR entering a "cease mode."

A. *Extended Operation in Cease Mode—October 2018*

This event illustrates how a large IBR remained in cease mode for an extended duration, i.e., 10 seconds, following a voltage depression caused by a phase-to-phase fault on the interconnecting line. This prevented local line protection from operating and created a risk of out-of-synchronism reclosing,

compromising the safety and reliability of the facility and the grid.

As shown in Fig. 32, this event occurred on a short 132 kV radial transmission system connecting a 102 MW Type IV wind generation facility, comprising 34 units rated at 3 MW each. A tree contact on the short transmission line linking the wind facility to a utility switching station triggered a Phase-C-to-A fault.

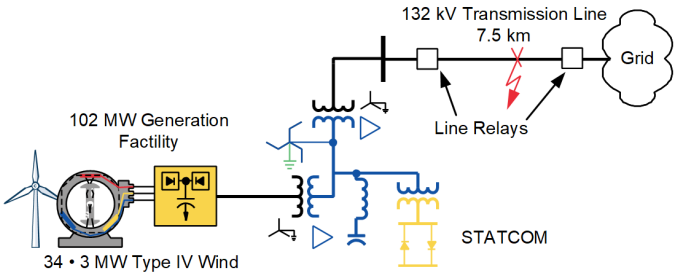

Fig. 32. A 132 kV radial transmission network integrating a Type IV wind generation facility

Prior to the fault, the wind farm exported ~100 MW at unity power factor. Fig. 33 compares the three-phase current waveforms recorded by protective relays on both the utility and IBR sides, preprocessed using a 60 Hz bandpass filter.

a) The utility side displays conventional synchronous generator behavior with high-magnitude, equal-and-opposite currents in the two faulted phases. The distance protection operated correctly, tripping the breaker and issuing a DTT to the wind facility.

b) The wind facility side displays that the converter-based system reduced current immediately upon fault detection, dropping to near-zero in just two cycles, in stark contrast to the expected fault response.

1) Protection System Failures on the IBR Side

The protection element on the IBR side either failed or incorrectly asserted, compromising protection reliability due to extended cease mode operation:

- The phase distance element at the IBR terminal did not operate. The apparent loop impedance landed outside the mho characteristic, dynamically expanding into the second, instead of the traditional third, quadrant.
- LOP logic asserted due to minimal change in current and a substantial voltage drop, further inhibiting distance element operation.
- 32QF asserted because the relay was configured to default to the forward direction (for dependability) upon detecting an LOP condition.

Unfortunately, the DTT signal was miswired, leaving the wind facility energized in cease mode.

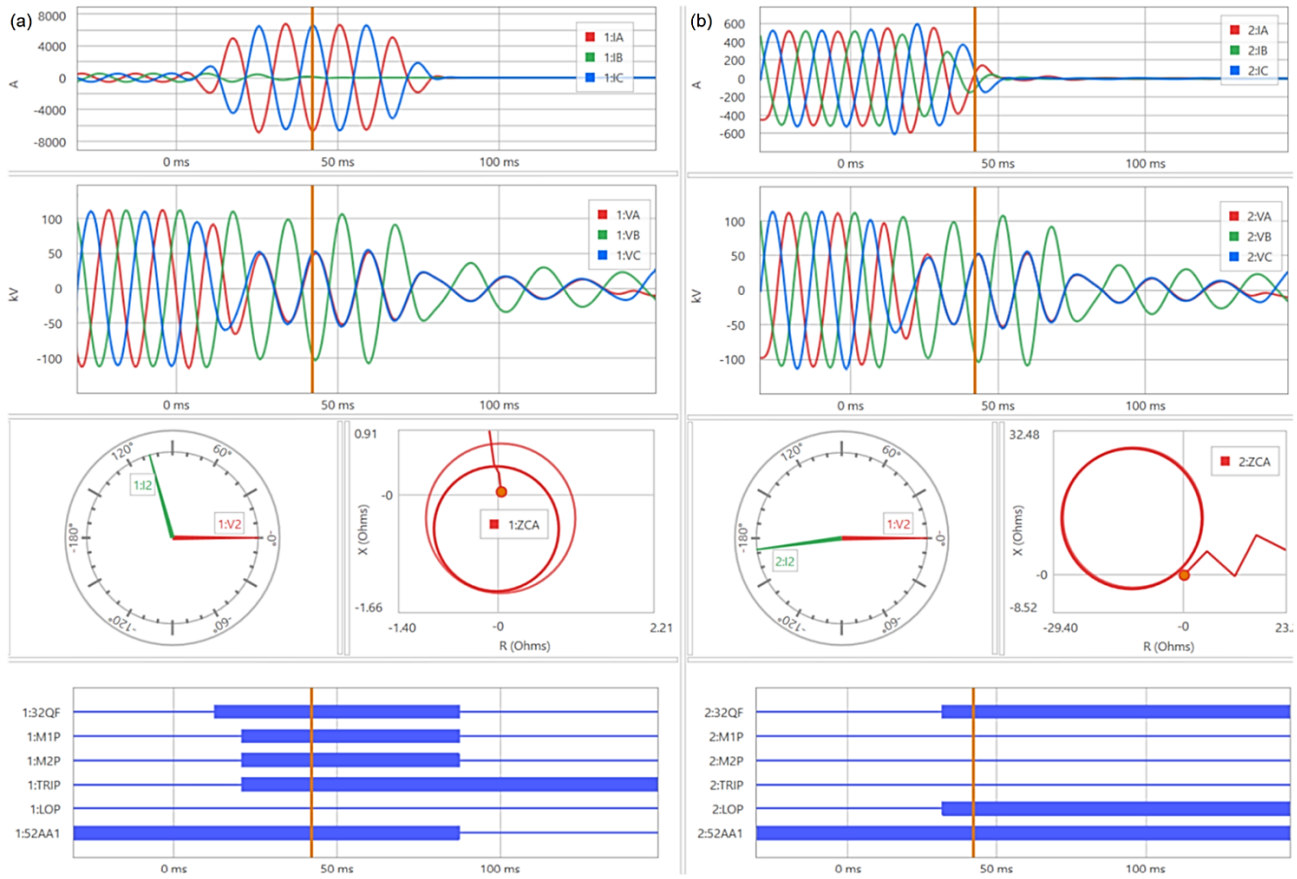

Fig. 33. Line protective relay recordings from a) the grid b) the IBR

2) Risk of Out-of-Sync Closing

From other event reports and sequence-of-event data (not shown here) the facility's converter remained in cease mode for approximately 10 seconds after the fault. When the cease mode cleared, the IBR attempted to re-energize the line in grid-following mode. Due to the lack of grid voltage reference, this led to voltage collapse.

At the same moment, the utility-side autorecloser, also configured with a 10-second dead-line interval, attempted to reclose. This narrowly missed an out-of-synchronism closing, which could have damaged both utility and IBR equipment.

Eventually, time-delayed undervoltage backup protection operated, isolating the wind facility from the grid.

B. *Inconsistent Operation in Cease Mode—August 2020*

This event demonstrates that even when IBRs experience the same grid disturbance, their responses in cease mode can vary significantly depending on the inverter manufacturer and associated control algorithms.

The incident occurred on a transmission system involving 230 kV and 500 kV networks (see Fig. 34), where two solar generation facilities were integrated:

- Facility 1: 154 MW solar plant.
- Facility 2: 134 MW solar + 60 MW battery energy storage system (BESS).

Both facilities were connected to the same 230 kV bus but through separate interconnection lines. Each site used smart IBRs configured to meet prevailing interconnection standards.

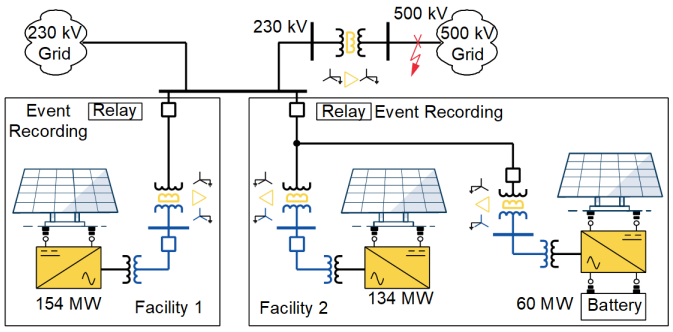

Fig. 34. A utility transmission system, 230 kV and 500 kV, integrating two IBR facilities

A Phase-B-to-ground fault occurred upstream on the 500 kV system. Fig. 35 captures the markedly different fault current responses from the two facilities immediately after the fault was cleared. Fig. 35(a) and Fig. 35(b) display the three-phase currents from Facility 1 and Facility 2, respectively. Fig. 35(c) and Fig. 35(d) display the three-phase voltages, measuring identical voltages at the shared 230 kV bus by Facility 1 and Facility 2.

During the fault, the Phase B voltage (VB) remained higher than 85 percent of the nominal, i.e., the voltage at the IBR terminals did not drop significantly. Both facilities continued injecting close to pre-fault current levels during the fault, which was cleared in approximately 50 ms by primary protection, followed by differing responses from the two facilities:

- **Facility 1** showed a slight reduction in current output between 70–140 ms, after which it resumed injecting its pre-fault current.
- **Facility 2** entered momentary cessation at around 50 ms and remained in that state until approximately 100 ms. Although it began ramping up its output thereafter, its current remained lower than pre-fault levels through the end of the event (1.8 s, not shown).

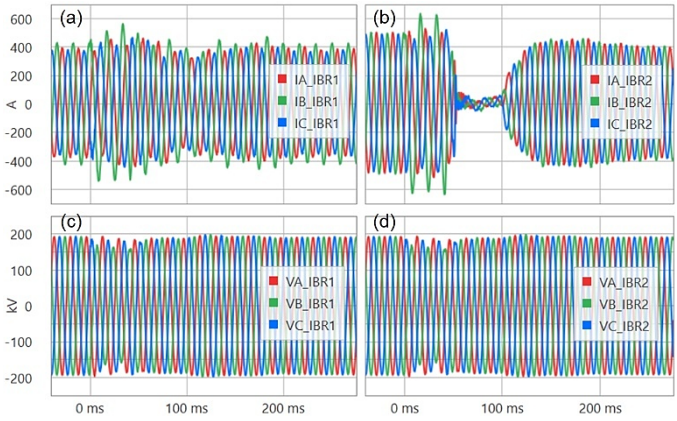

Fig. 35. Fault responses of two IBR facilities connected to the same 230 kV bus: a) Facility 1 current response, b) Facility 2 current response, c) Facility 1 measured voltages, and d) Facility 2 measured voltages

This event revealed Facility 2's non-compliance with grid code requirements and exposed inconsistencies in dynamic performance between the two IBR sites. Although both were designed to meet the same interconnection requirements, their actual field behaviors differed due to different implementations.

C. *Camouflaged Cessation—April 2024*

This event highlights how a momentary cessation by an IBR during a grid disturbance can be masked by transformer I_0, potentially leading to misinterpretation of IBR behavior. The cessation was only revealed after removing I_0 from the phase currents.

The event occurred at a 350 MW solar PV and BESS facility interconnected to a 230 kV transmission system shown in Fig. 36. A Phase-B-to-ground fault occurred on the transmission system, and primary protection cleared the fault in two cycles.

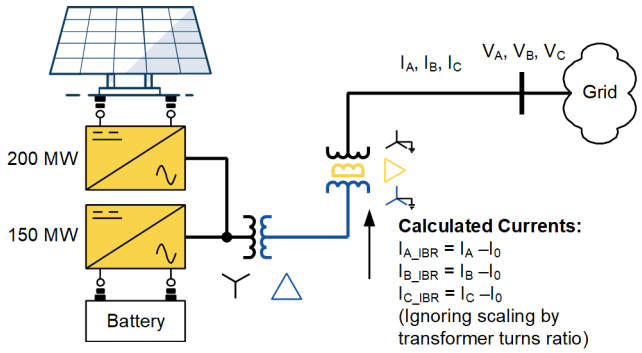

Fig. 36. 350 MW Solar PV and BESS facility

Fig. 37 presents captured oscillography, showing:

- **Top panel:** Three-phase bus voltages at the 230 kV IBR point of interconnection. The modest sag confirms the fault was remote.
- **Middle panel:** Three-phase currents injected into the bus by the IBR facility during the event.
- **Bottom panel:** The raw three-phase currents minus the raw I_0.

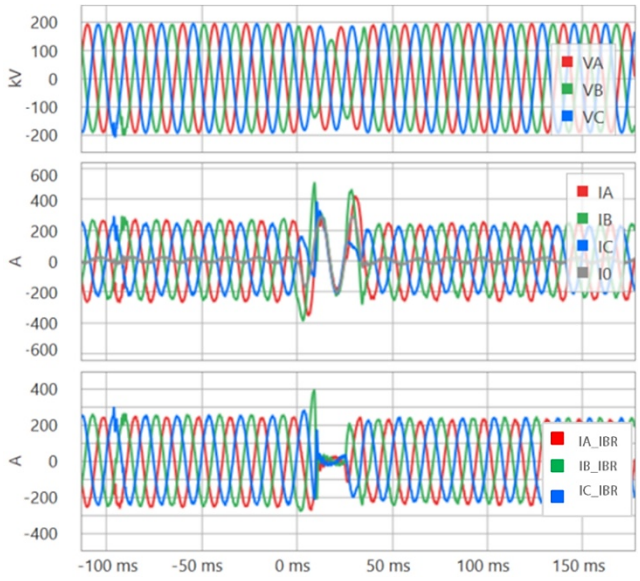

Fig. 37. Zero-sequence current from the transformer camouflaging the cease mode

The facility was grounded through a transformer configuration that allowed I_0 to flow during the fault. Initially, the large apparent current suggested the IBR remained online and injected reactive current for voltage support. However, after removing I_0, the corrected waveform revealed that the IBR actually entered momentary cessation for approximately one cycle, injecting negligible current.

D. Partial Cease Mode or Reduced Fault Current

It is well known that IBRs are designed to limit their short-circuit current response to approximately 1.0 to 1.3 pu of their facility rating to protect their sensitive power electronic components. This subsection examines two events where protection devices were deliberately programmed with sensitive triggering thresholds to capture detailed event records. These records enhance our understanding of IBR short-circuit current behavior and their response to voltage depressions during system disturbances.

An instantaneous phase undervoltage element, set at 95 percent of nominal voltage, was used as the sensitive trigger. When this undervoltage element is applied at a strong bus, it can capture events caused by faults one or two terminals away. When applied at a weak bus, it can detect faults located even farther, typically three or more terminals away.

1) Remote Phase-to-Ground Fault—June 2024

Fig. 38 presents a one-line diagram of a radial 230 kV transmission line serving three independent IBR facilities. These facilities include a combination of solar PV, BESS, and shunt capacitors. The configuration and ratings are as follows:

- **Facility 1:** 250 MW solar PV
- **Facility 2:** 166 MW solar PV, 180 MW BESS, 28 MVAR shunt capacitors
- **Facility 3**: 274 MW solar PV, 300 MW BESS, 64 MVAR shunt capacitors.

The aggregate installed generation capacity is 1170 MW:

- Solar PV: 690 MW
- BESS: 480 MW
- Total shunt capacitors: 92 MVAR

The full-load or 1 pu current for the radial 230 kV line is approximately 2,900 A.

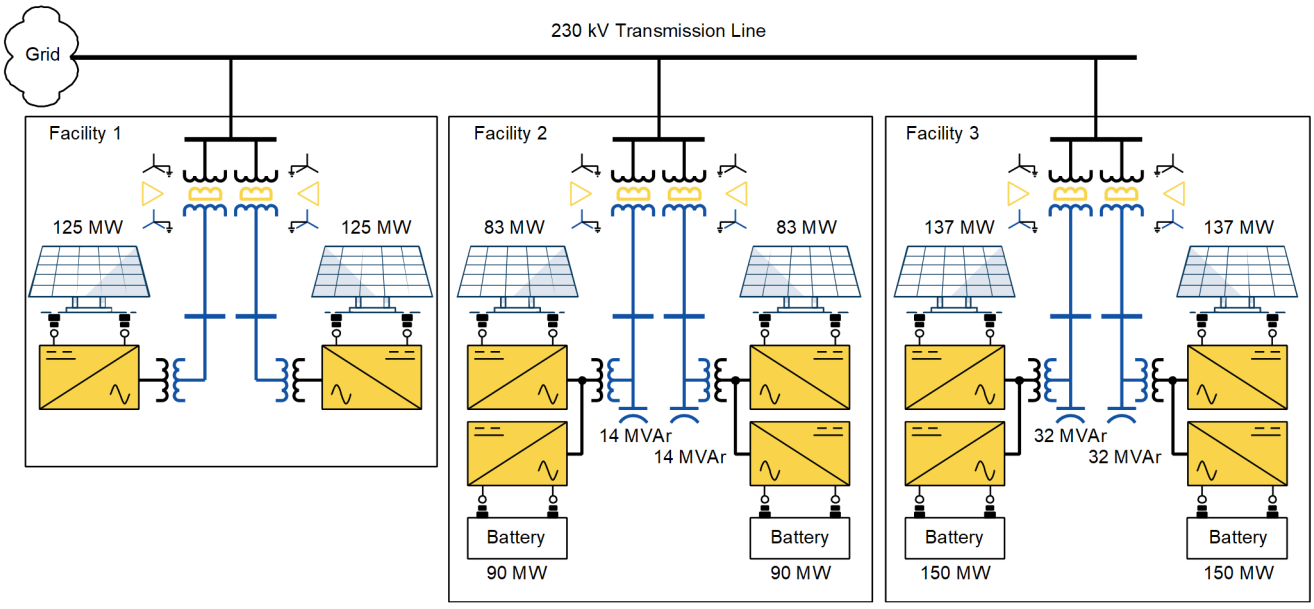

Fig. 38. 230 kV radial line with three IBR facilities

Sensitive undervoltage event triggers were implemented at the grid-side breakers to capture system disturbances and analyze IBR dynamic response. This monitoring setup proved effective, resulting in multiple high-resolution relay records for external faults on a remote 500 kV line.

Fig. 39 shows the IBRs' responses to a permanent single-phase-to-ground fault about 40 miles away from the station on a 500 kV transmission line. The 500 kV transmission line had high-speed protection and reclosing, clearing the fault in about three cycles and ensuing autoreclose after 500 ms on the permanent fault. The three phase currents in the figure are the sum of the currents from the three IBR facilities. The three phase voltages are measured on the 230 kV bus.

For the initial fault, the minimum phase voltage dropped to 0.73 pu. I_0 is filtered out from the phase currents and shown in the bottom panel in Fig. 39. It appears that the IBR current increased from 680 A (0.23 pu) to 945 A (0.33 pu) for half a cycle. The current output then decreased to 560 A (0.19 pu) before entering into complete cease mode during the fault.

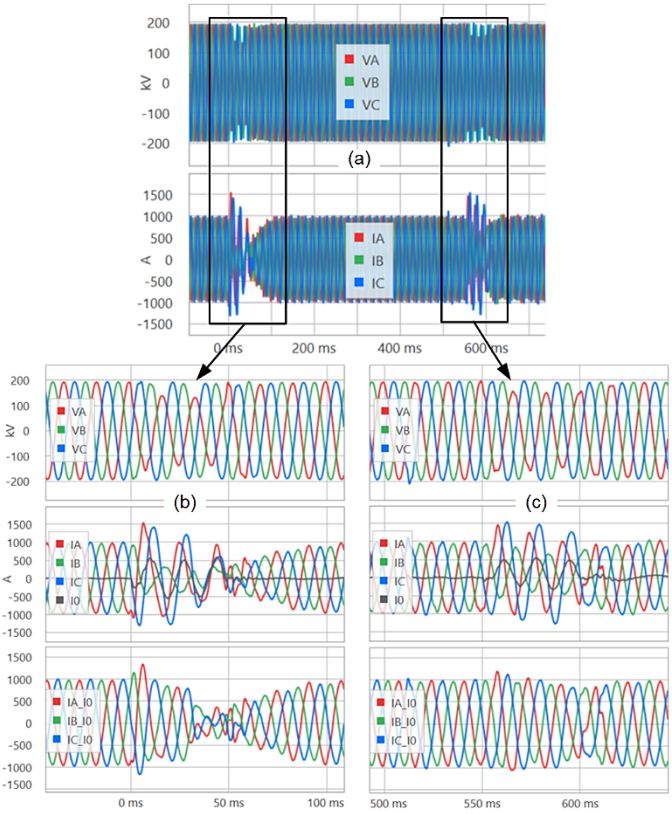

Fig. 39. Remote ground fault response of IBR facility showing a) the overall record, b) the initial fault, and c) the high-speed reclose

Following the autoreclose that occurred 0.5 seconds later, the maximum IBR current output was 840 A (0.29 pu), and the IBR remained in the partial cease mode for the same fault location. Based on the installed generation and rated current, the expected IBR fault current response was approximately 1.3 pu. However, the actual contribution was significantly lower, confirming that IBRs did not deliver the expected short-circuit current response under fault conditions.

2) Close-in Phase-to-Ground Fault—February 2024

Fig. 40 illustrates the response of the same IBR facilities shown in Fig. 38 during a more severe phase-to-ground fault. The fault occurred on the same 500 kV transmission line as the previous event but was located approximately one mile from the 500 kV/230 kV station. During this fault, the Phase A voltage dropped significantly to about 0.34 pu. A notable increase in the IBR's Phase A and Phase B currents was observed, reaching a maximum of approximately 0.7 pu.

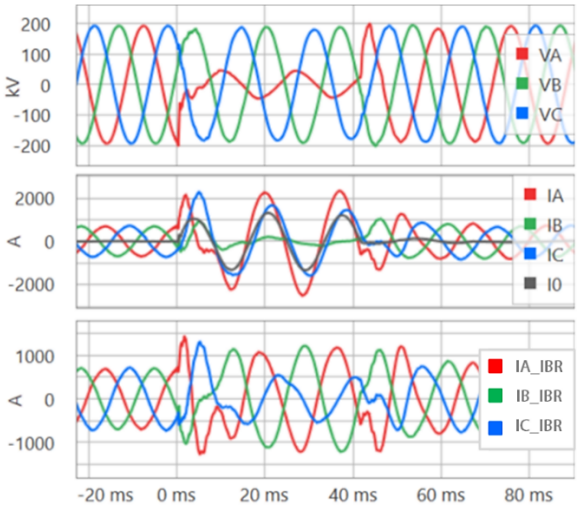

Fig. 40. Close-in ground fault response of IBR facility

This event occurred early in the morning, around 6:30 a.m., when the solar facilities were not generating. With all the BESSs still online and assumed to have a sufficient state of charge, the expected short-circuit response from the BESSs should have been approximately 1.3 pu (or 1,560 A) based on a rated continuous current of 1,200 A. However, the actual current contribution from the BESS was only about 860 A (0.7 pu).

This event further demonstrates the tendency of IBRs to enter partial cease mode or to otherwise underperform during fault conditions, failing to deliver the anticipated 1.3 pu current even during severe, close-in faults.

E. Cease Mode Implications and Protection Challenges

The cease mode feature in IBRs is designed to protect power-electronic converters by allowing the resource to ride through system voltage depressions caused by external disturbances without overstressing its components. However, a critical downside is that it disables reactive power support at the precise moment it is most needed, when the system voltage is depressed, posing a risk to overall voltage stability. Additionally, in cease mode, it may seem that the IBR is disconnected, which might defeat dead-line supervision and introduce a risk of out-of-sync reclosing.

Many modern grid codes and standards, including those aligned with PRC-029-1 [11] and IEEE Std 2800 [2], explicitly prohibit the use of cease mode during faults and instead require IBRs to support the grid by injecting reactive current during voltage depressions. In practice, however, zero-sequence paths presented by transformers can obscure the true dynamic response of IBRs. By removing I_0 from the recorded fault

current waveforms, analysts can better assess whether the IBR response aligned with the required ride-through performance.

A detailed understanding of IBR behavior under various fault conditions is essential to properly apply protection settings. The most challenging scenario occurs when IBRs enter cease mode and fully shut down current injection. Conventional protection schemes rely on fault current magnitude for detection and isolation. When IBRs provide little or no current during faults, these schemes can fail to operate reliably.

Protection engineers typically design settings based on an assumed IBR fault current contribution in the range of 1.0 to 1.3 pu of rated output. However, the events described in this section show that IBRs can fail to meet this expectation due to partial or full cease mode operation. As a result, protection settings based on these assumptions may not provide dependable performance, undermining system reliability, power quality, and safety.

VI. Unintentional Islanding Challenges

This section presents events that illustrate the rapid decline in the frequency of unintentional islanded networks due to low-inertia IBRs, which degrade the voltage measurements and corrupt the expected protection operating times.

Traditional distribution systems were designed for unidirectional power flow, with the primary purpose of serving local loads. Many such systems are tapped from the transmission grid through ungrounded transformers (e.g., delta connection on the high side), which inherently block I_0 flow from the distribution side back into the transmission system.

However, the modern electric grid has undergone a major transformation. Distribution systems are increasingly hosting distributed generation resources, ranging from small rooftop solar installations to dedicated multi-megawatt facilities. This shift has introduced system conditions that transmission systems were not originally designed to handle.

One critical consequence is the unintentional islanding of transmission lines with ungrounded resources. Following a single-line-to-ground fault, the transmission line may trip and isolate itself from the grid, but the resources in the distribution system remain connected via the transformer. Depending on the load-to-generation ratio within the islanded section, the transmission line can remain energized with elevated voltages on the healthy phases.

Although the connected resources contribute to negligible ground fault current because of the ungrounded transformer configuration, their continued operation poses significant safety and equipment risks, including wildfire ignition in dry environments and overstress of surge arresters on healthy phases. Timely detection and disconnection of these islanded resources is critical to system safety.

IEEE Std 1547-2018 mandates that distributed energy resources (DERs) shall disconnect within two seconds using anti-islanding protection [12]. However, in some jurisdictions, particularly those with wildfire risk or sensitive infrastructure, this time frame is considered too slow.

One effective mitigation strategy is to employ DTT from the transmission terminal to the connected DER. While DTT provides fast and reliable isolation, it is often cost-prohibitive for small-scale generators due to the need for dedicated communications infrastructure. As a practical alternative, the applications discussed in this section deployed time-delayed zero-sequence overvoltage (59G) and healthy-phase overvoltage (59P) detection logic to initiate DER tripping [13].

A. Degradation of Voltage Measurements—October 2022

As shown in Fig. 41, a 6 MVA solar facility and local distribution loads were tapped into a utility's 70 kV sub-transmission system via an ungrounded transformer [14].

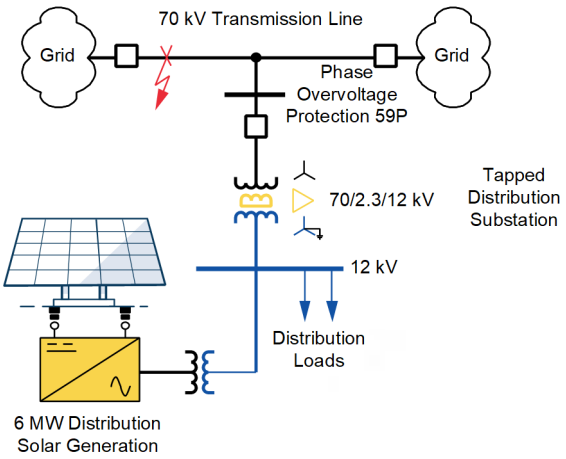

Fig. 41. IBR tapped into the sub-transmission system via an ungrounded transformer

A ground fault on the 70 kV line initiated a sequence of tripping actions. The grid-connected terminals opened, isolating the line from the grounded system. However, the solar facility remained connected and energized, now operating in an ungrounded, islanded condition. In this case, no DTT scheme was deployed. Instead, the overvoltage relay, located at the 70 kV tapped bus, was configured with two levels of healthy-phase overvoltage protection:

- **Level 1** (59A1, 59B1, 59C1): 150% of nominal voltage with a 4-cycle delay.
- **Level 2** (59A2, 59B2, 59C2): 120% of nominal voltage with a 20-cycle delay.

During a single-line-to-ground fault, after grid disconnection, the two healthy phases are expected to rise to 173 percent of nominal voltage (i.e., $\sqrt{3}$ • base voltage). Hence, both settings provided adequate detection margins. Yet in the actual event, the relay failed to trip.

1) Overvoltage Response During an Islanded Fault

Fig. 42 presents the recorded three-phase voltage waveforms during a Phase-C-to-ground fault on the islanded 70 kV line. The healthy phase voltages rose as follows:

- Phase A voltage rose to 142% (81 kV peak)
- Phase B voltage rose to 162% (92 kV peak)

These clearly exceeded the Level 2 threshold of 120 percent, yet they did not remain asserted firmly.

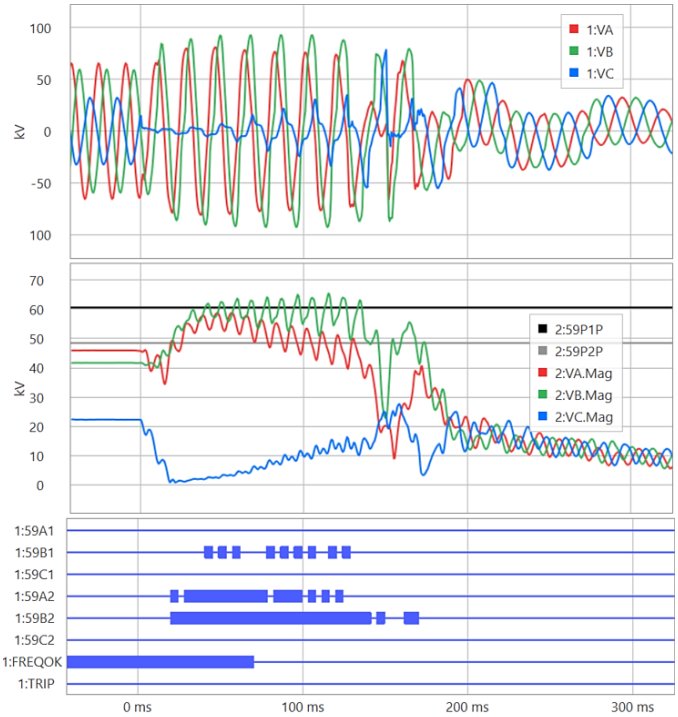

Fig. 42. Three-phase voltages at the 70 kV tapped bus during a Phase-C-to-ground fault with an ungrounded IBR connected but isolated from the grid

Although the voltages elevated significantly, the phasor magnitudes calculated by the relay exhibited substantial oscillations. This caused the overvoltage elements to chatter (i.e., repeatedly pick up and drop out), preventing a stable trip condition.

2) *Rapid Frequency Decline Degrading Voltage Measurements*

To investigate further, the waveform data were exported to MATLAB, and the frequency was calculated using zero-crossing analysis of the voltage waveform. The alpha voltage ($V\alpha = VA - 0.5 \cdot VB - 0.5 \cdot VC$) was used to remove any common-mode zero components in the voltages.

Fig. 43 shows that the frequency dropped rapidly from 60 Hz to 56.7 Hz, with a ROCOF exceeding 60 Hz/s. The fast ROCOF can be attributed to:

- Generation-load unbalance in the islanded network.
- Lack of frequency control by low-inertia, grid-following IBR.

Most digital relays track frequency using bandpass filters tuned around 60 Hz. The relay used in this event could track frequency changes up to 20 Hz/s. Beyond that, it reverted to a fixed 60 Hz estimation. Therefore, the high ROCOF exceeded the relay's tracking capability and degraded its filtering performance.

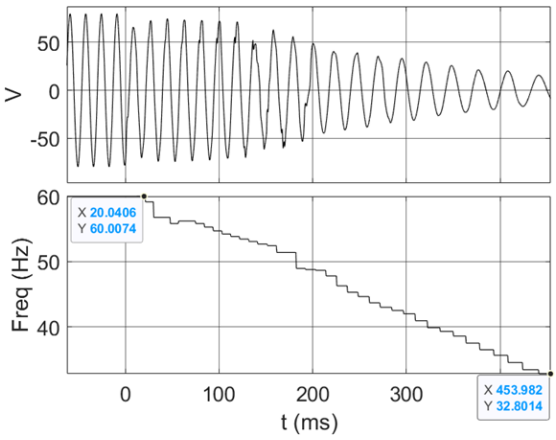

Fig. 43. Fast ROCOF of an islanded IBR

3) *DFT Filter Behavior and Magnitude Attenuation*

Fig. 44 illustrates the response of a Discrete Fourier Transform (DFT) filter under different input frequencies. While the 60 Hz input produces a stable output, inputs at 55 Hz and 50 Hz exhibit oscillatory responses. Furthermore, the magnitude of the 50 Hz signal is significantly reduced due to the filter's attenuation. The oscillatory behavior and attenuation at off-nominal frequencies can significantly compromise the overvoltage element's dependability.

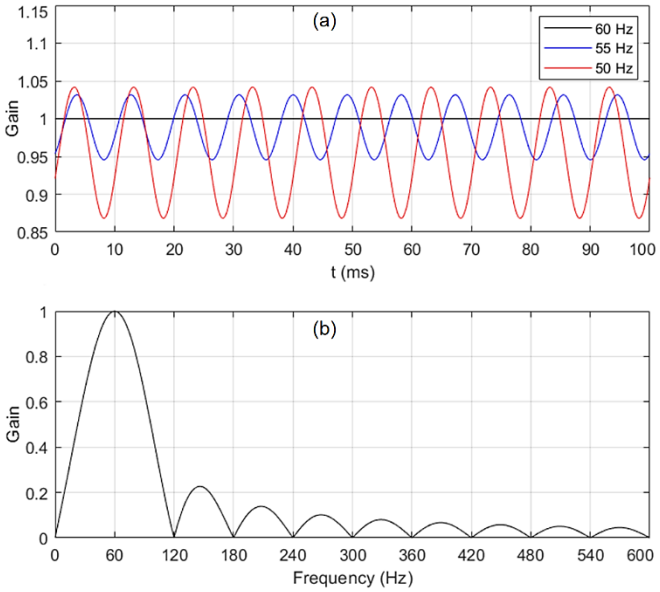

Fig. 44. Response of a 60 Hz DFT-based bandpass filter to a) 60 Hz, 55 Hz, and 50 Hz signals and b) the mean gain at different frequencies

B. *Time-Delay Corruption—May 2025*

This event further illustrates the impact of high solar penetration in the distribution system, which contributed to elevated voltages in the islanded transmission system following the loss of grounding. However, due to a rapid decline in system frequency, the voltage-based protection element experienced unexpected, longer delays.

Fig. 45 depicts a 70 kV transmission line feeding three tapped distribution substations, one of which has a transformer presenting a path for zero sequence.

- **Substation 1:** This substation hosts a distribution-connected solar generator and local loads. Its transformer does not provide a ground reference to the transmission system. A 70 kV overvoltage relay is installed to trip the distributed generation during abnormal conditions.
- **Substation 2:** Serves many residential customers with rooftop solar systems. Like Substation 1, its transformer is also ungrounded on the transmission side and includes 70 kV overvoltage protection to trip the solar feeder circuits.
- **Substation 3:** Supplies only load (no generation) and provides a solid ground reference to the transmission system through its transformer configuration. It is equipped with a transfer switch to source power from an alternate grid supply after transmission faults.

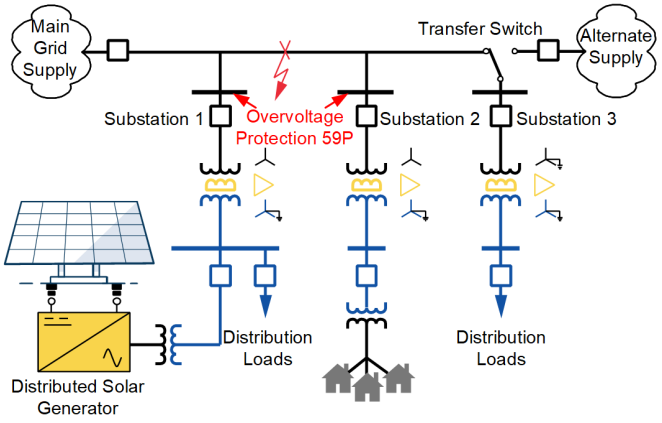

Fig. 45. Rooftop solar and a distributed solar generation connection to the transmission system

1) Sequence of Events

A ground fault occurred on the transmission line. Line protection operated as expected, tripping the breaker and islanding the three substations along with their connected distributed generation. Because Substation 3 was still connected, providing effective grounding, no overvoltage occurred immediately on the 70 kV system.

However, following the fault, the automatic transfer switch at Substation 3 activated, connecting it to the alternate supply source and removing the only effective ground reference from the islanded portion of the transmission system.

Fifteen seconds later, the main transmission breaker autoreclosed. The line was initially healthy. Within minutes, however, the original fault reignited, causing the breaker to trip again. This time, the transmission system lacked a zero-sequence reference because Substation 3 was now transferred to the alternate supply. Despite this, the line remained energized by distributed and rooftop solar generation, causing the system neutral to float and resulting in significant phase-to-ground overvoltages.

2) Overvoltage Recording

Fig. 46 illustrates overvoltages recorded by two identical, redundant protection systems monitoring the 70 kV bus at Substation 2. The phase-to-ground voltage reached a maximum of 69.3 kV (1.7 pu), triggering the overvoltage protection scheme in 356 ms and causing the disconnection of all rooftop solar generators connected to that substation.

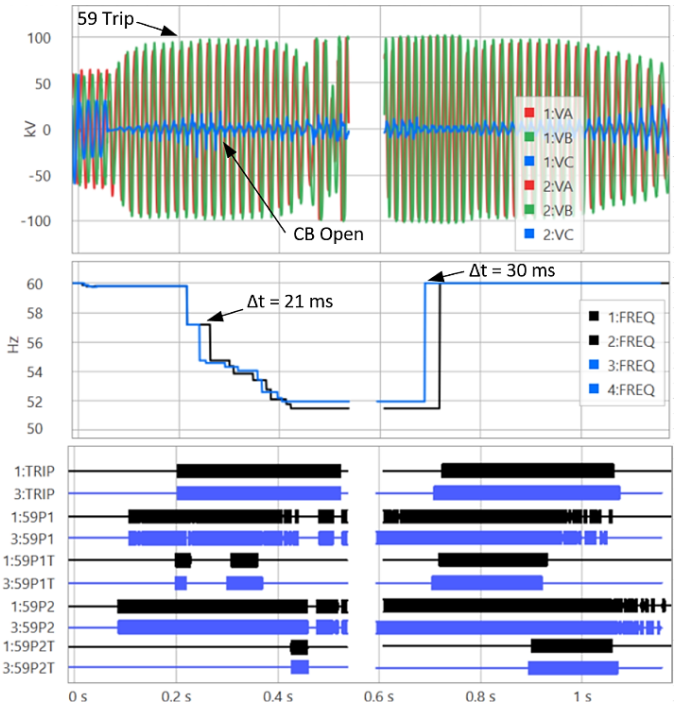

Fig. 46. Overvoltages recorded at Substation 2

However, the overvoltage condition on the 70 kV system persisted for approximately one second due to continued power injection from distributed solar generation at Substation 1, where the protection system failed to trip.

At Substation 1, the overvoltage relays were found to be non-operational, and the distributed generation continued to sustain the elevated system voltage for an extended period before eventually shutting down.

3) Operating Time Corruption Due to ROCOF

Post-event analysis revealed that the actual relay operating time differed from the expected value due to frequency deviations in the island network.

The overvoltage element was configured with a time delay of 20 cycles, which is 333 ms based on the nominal frequency of 60 Hz. However, the relay operated in 356 ms, which corresponds to 21.4 cycles at 60 Hz.

This discrepancy was caused by a rapid decline in frequency after the islanding event. The low-inertia solar generation resulted in a high ROCOF. Importantly, the relay computed the operating time based on the actual frequency of the measured voltage signal, not the nominal 60 Hz.

As a result, the lower measured frequency increased the real-world operating time, delaying trip operation beyond the originally intended configuration of 333 ms.

C. *Protection Degradation in an Islanded IBR Network*

Modern digital relays, including those with adaptive filtering, were originally designed for systems dominated by synchronous generators, where high inertia ensured gradual frequency changes. In contrast, IBRs lack inherent inertia and frequency control, leading to abrupt frequency shifts, particularly in islanded conditions.

Following grid disconnection, a system islanded with grid-following IBRs experiences a rapid frequency decline, often exceeding the frequency tracking capabilities of traditional relay algorithms. This can cause overvoltage protection to misoperate or fail to operate entirely, as relay phasor estimation becomes unstable during fast transients. The use of protection timers that do not reset instantaneously can help improve dependability.

A related issue arises from how relays interpret time-delay settings expressed in cycles. While engineers often assume these delays correspond to fixed durations at 60 Hz, many relays calculate delay based on the measured system frequency, meaning:

- If the frequency drops lower than 60 Hz, the relay takes longer to operate than expected.
- If frequency rises higher than 60 Hz, the relay operates sooner than expected.

This behavior can significantly impact protection timing in low-inertia IBR networks and must be accounted for in coordination studies and relay programming.

VII. Overexcitation and Subsynchronous Oscillations

This section presents three events that illustrate the unusual behavior of IBR control systems. These systems cause overfluxing in transformers and trigger subsynchronous oscillations.

A. *Transformer Overexcitation—August 2024*

This section presents an event in which the 34.5/500 kV interconnecting transformer became overexcited shortly after a 500 kV fault, causing a BESS facility with inverters along with the transformer to become disconnected from the grid.

In the system shown in Fig. 47, there was a Phase-B-to-ground fault on a 500 kV tie line connecting to a 400 MW BESS facility. The tie-line current differential protection tripped the BESS offline. After the tie-line trip, the inverters attempted to boost the terminal voltage (instead of shutting down), as shown in Fig. 48. There was also a decrease in frequency from 60 Hz to 58.8 Hz. The increased voltage and reduced frequency together resulted in a substantial increase in volts per hertz (V/Hz), which caused the 34.5/500 kV interconnection transformer to overexcite. The bipolar current spikes, which are characteristic waveforms of overexcitation, are evident in Fig. 48. The voltages and currents were severely distorted and had high harmonic components. The condition lasted longer than three seconds, even though one might expect grid-following IBRs to have shut down earlier.

Moderate overexcitation, as seen in the later part of this event, can cause overheating and dielectric stress, eventually degrading insulation. Damage from moderate overexcitation can occur within tens of seconds to minutes. Severe excitation, as seen in the earlier part of this event, can additionally break down interlaminar insulation, followed by rapid localized core melting and failure [15]. Damage from severe overexcitation events can occur within seconds.

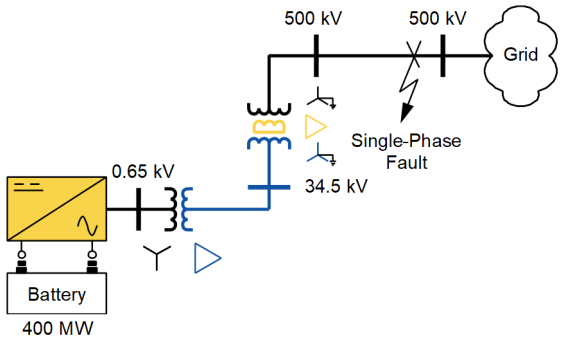

Fig. 47. Simplified one-line diagram of a 400 MW BESS connected to a 500 kV line that had a ground fault

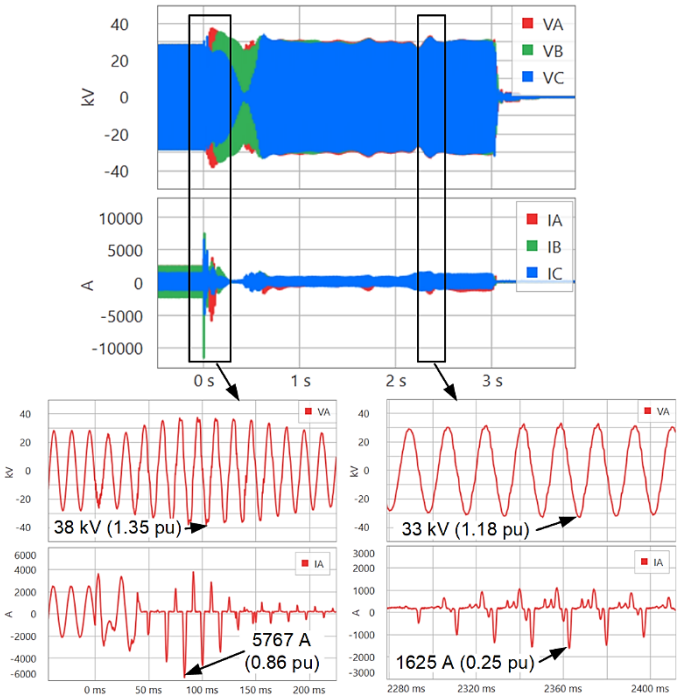

Fig. 48. Overexcitation oscillography following islanding.

B. *Subsynchronous Oscillation—September 2017*

This event corresponds to a subsynchronous oscillation (SSO) condition in southern Texas [16]. Referring to Fig. 49, a Phase-B-to-ground fault occurred on the transmission line connecting Station 2 to Station 3 [17]. The fault was cleared by the primary protection within 3 cycles. After the line tripped, the Type III wind generators in Plants 1 and 2 became radially connected with the series capacitors on the line connecting Station 3 and Station 4. The interaction between the series capacitors and IBR controls subsequently caused the SSO condition. The event was investigated, and it was determined that the SSO ceased when the IBR tripped. While the SSO condition has been thoroughly investigated in literature [16], little is known about what contributed to the IBR plant trip that helped save the system from prolonged oscillations. It

happened to be a misoperation of a transformer differential relay.

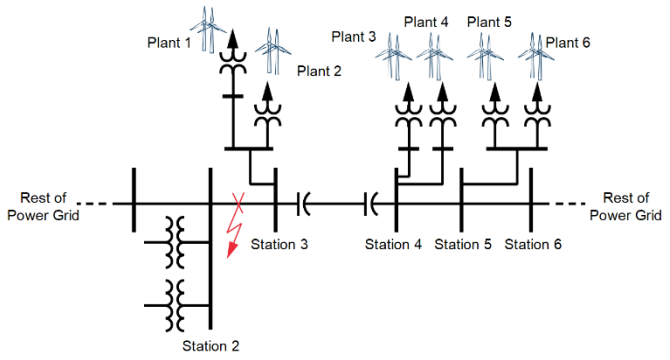

Fig. 49. One-line diagram for a 2017 southern Texas SSO event

The phase currents from the low-voltage winding (IpW1) and high-voltage winding (IpW2) measured by the Plant 1 transformer relay are shown in Fig. 50(a) and Fig. 50(b), respectively. This relay did not have voltage measurements available and volts-per-hertz protection was not applied. Fig. 50(c) to Fig. 50(e) show the compensated and normalized phase currents from the two windings. The method of compensation for the Winding 1 current is shown in (1). When there is a significant difference between the two winding currents (I1W1 – I1W2), differential element 1 (87R1) operates.

$$I1W1 = \frac{IAW1 - IBW1}{\sqrt{3} \bullet TAP1} \quad (1)$$

where:

I1W1 = Compensated Differential Element Current 1 from Winding 1

IAW1 = Phase A Current from Winding 1

IBW1 = Phase B Current from Winding 1

TAP1 = Scaling factor to normalize Winding 1 current

Referring to Fig. 50(c) through Fig. 50(e), there was no differential current during the Phase-B-to-ground fault (cleared in 42 ms) and the transformer differential protection restrained correctly. After the fault cleared, the SSO condition was triggered, resulting in elevated line voltages. The line relay recordings of Fig. 51 show that the voltage reached a maximum of 2.45 pu at a significantly low frequency, approximately 25 Hz. This low-frequency overvoltage caused overexcitation of a network transformer. The resulting excitation current from the overexcited transformer appeared as a differential current, as seen in Fig. 50(c) through Fig. 50(e), across all three compensated and normalized differential channels.

Notably, this overexcitation current was at a subharmonic frequency of approximately 25 Hz, rather than the nominal system frequency of 60 Hz. Differential protection is typically blocked during transformer overexcitation via fifth-harmonic blocking elements (5HBn), and V/Hz protection is instead relied upon to protect the transformer from damaging overexcitation. However, this case presented a unique scenario because two dominant frequency components were present, complicating the protective relay response. Fortunately, or unfortunately, the fifth-harmonic blocking did not assert, and the differential protection operated. This response helped suppress the SSO, though it technically constituted a protection misoperation. Even if volts-per-hertz protection had been applied, it may not have responded effectively due to the multi-frequency nature of the event.

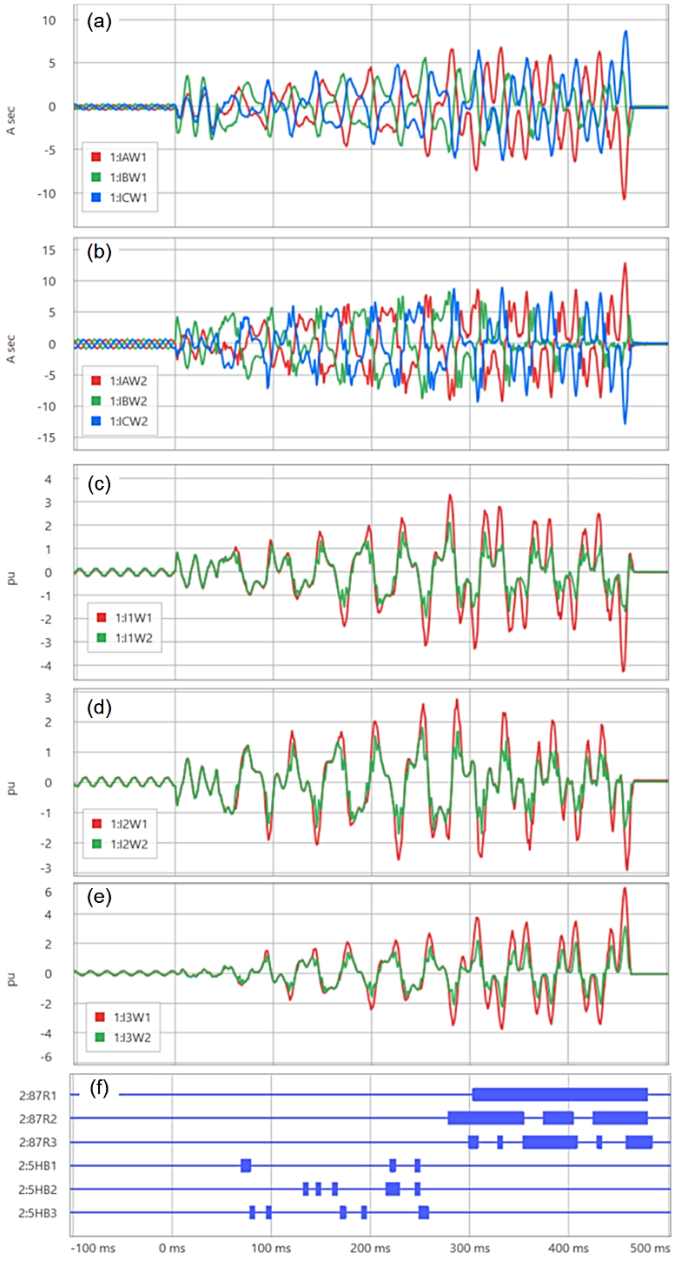

Fig. 50. Subharmonic overexcitation captured by a transformer differential relay: a) 354 kV Winding 1 phase currents, b) 34.5 kV Winding 2 phase currents, c) Compensated Current 1, d) Compensated Current 2, e) Compensated Current 3, and f) the transformer differential element response

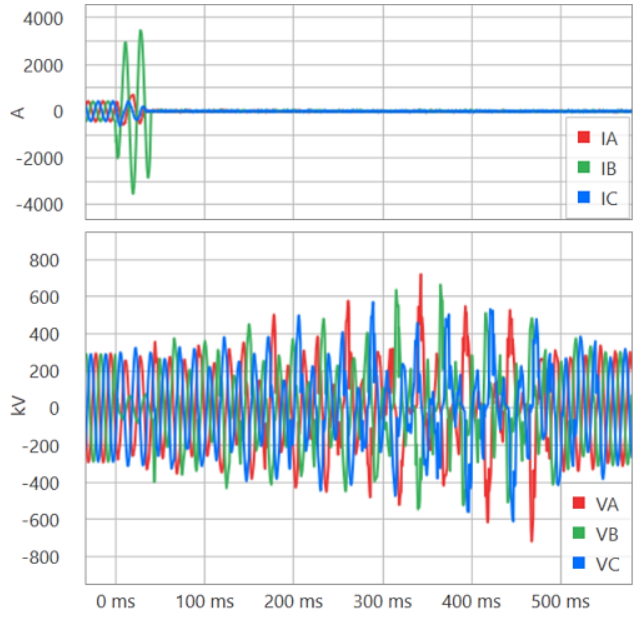

Fig. 51. Subharmonic 2.45 pu overvoltage on a 345 kV line due to SSO

C. *Forced Subsynchronous Oscillations—July 2025*

This event demonstrates a forced SSO condition, apparently triggered by the control system of a 300 MW solar facility under unknown circumstances. The facility was connected to a strong grid, with short-circuit strength exceeding 3,000 MVA and a short-circuit ratio (SCR) greater than 10.

Low-frequency oscillations were captured by line protective relays configured with sensitive undervoltage settings. As illustrated in Fig. 52, the solar facility's output repeatedly ramped from approximately 4 MVA to 180 MVA every 0.15 seconds, sustained for nearly 1.5 hours. The oscillation frequency was approximately 6.7 Hz.

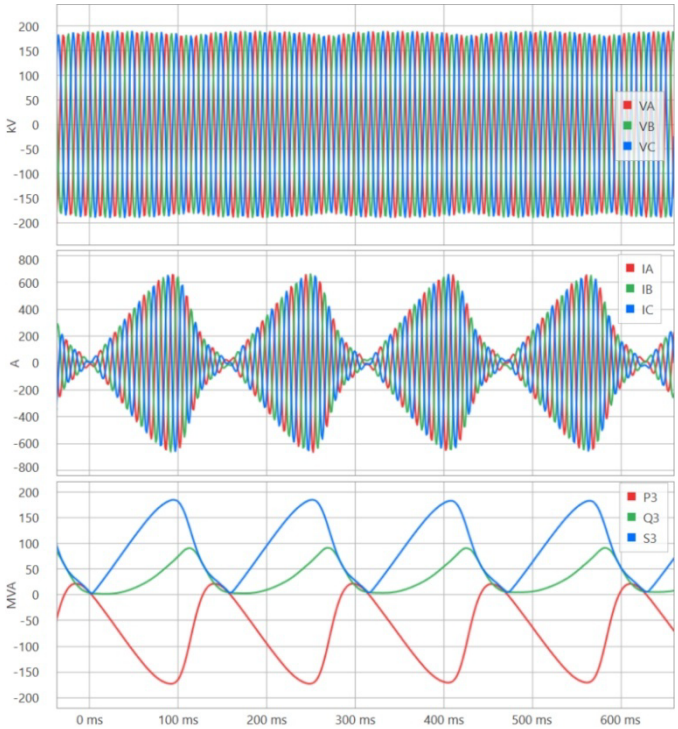

Fig. 52. Forced SSO introduced by the IBR controller in a new installation

According to NERC's classification [18], the likely causes for oscillations at the frequency bands are defined as follows:

- 0.01 to 0.15 Hz: Governor, plant, or automatic generation control.
- 0.15 to 1 Hz: Electromechanical inter-area and local plant oscillations.
- 1 to 5 Hz: Local plant/intra-plant modes, local generator control, excitation control, and dc circuit controls.
- 5 to 50 Hz: Torsional oscillations, SSO, fast-acting controllers.

Based on this classification, the observed 6.7 Hz oscillation qualifies as an SSO. This oscillation further fits the forced oscillation category described in [19].

The magnitude of the oscillation was significant. Real and reactive power fluctuations from the IBR facility were approximately 200 MVA. These power fluctuations caused voltage swings from 232 kV down to 218 kV, a 6 percent voltage sag in an otherwise strong system, thereby triggering event recorders. Importantly, no system faults were recorded during this interval.

Synchrophasor data analysis revealed that a nearby 500 kV STATCOM was also oscillating during this event. Preliminary investigations suggest that the solar facility and the STATCOM may have been dynamically interacting, resulting in coupled oscillations.

This incident highlights the critical importance of automated oscillation detection, classification, and source location using synchrophasor data. When oscillatory behavior like this emerges, rapid identification and mitigation are essential. With the ongoing proliferation of IBRs, such oscillatory events may become more common, underscoring the need for advanced monitoring and control strategies.

D. *Risks From Unusual IBR Control Behavior*

Grid-following IBRs are generally expected to shut down upon grid disconnection. However, in the first event, an IBR remained online, boosting terminal voltage while frequency declined, resulting in transformer overexcitation for over three seconds. This suggests the need for volts-per-hertz protection on transformers connected to IBRs, like practices used in synchronous generating plants [20]. Additionally, the use of voltage transformers (VTs) at the medium-voltage level can help ensure dependable volts-per-hertz protection. This is because the grid may be strong and not allow significant voltage changes at the high-voltage level.

The second event highlighted the risk of SSO when a Type III WTG operates radially into a series-compensated line. To prevent equipment damage, countermeasures such as SSO detection, capacitor bypassing, controlled WTG tripping, and improved transformer differential and volts-per-hertz protection are essential.

In the third event, an IBR control anomaly triggered a forced SSO, causing large power fluctuations and degrading power quality. Forced SSOs can propagate through the grid, inducing damaging oscillations and even causing equipment failure at

remote locations, posing a serious risk of wide-area disturbances.

VIII. Harmonics

This section presents a series of events illustrating unusual IBR control system behaviors during the steady-state or after disturbances. These behaviors caused inverter trips, posed a security threat to the protection systems, and risked breaker failures.

A. *Inverter Trip Due to Resonant Harmonic Overvoltage—March 2025*

Fig. 53 shows a simplified one-line diagram of a 250 MW solar facility interconnected to a strong utility system via a short (<0.1 mi) 345 kV line. The facility included two 10.8 MVAr shunt capacitors at 34.5 kV for voltage support at the 345 kV bus.

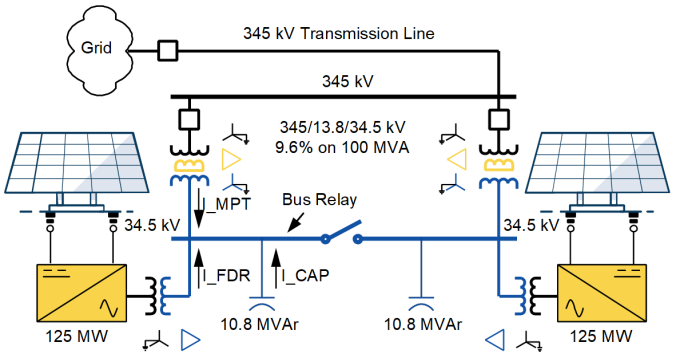

Fig. 53. Simplified one-line diagram of a 250 MW solar PV facility with shunt capacitors for providing voltage support

During capacitor control testing, a significant overvoltage occurred, causing inverters to trip offline. Fig. 54 presents the oscillography captured by the 34.5 kV bus relay, including solar feeder current (I_FDR), capacitor current (I_CAP), and main power transformer current (I_MPT), indicated in Fig. 53. The overvoltage was resonant in nature, occurring at approximately 592 Hz, just below the tenth harmonic.

The root cause is identified as a parallel resonance condition at the 34.5 kV bus, formed by the shunt capacitor and the leakage inductance of the 34.5/345 kV transformer. With a transformer leakage inductance of 3.03 mH and a capacitor bank capacitance of 24 µF, the system was tuned to a resonant frequency near 590 Hz, closely matching the frequency of distortion observed during the event.

Although the inverter was injecting less than 0.1 percent of the tenth harmonic (600 Hz), the parallel resonance circuit presented a high impedance near 590 Hz, significantly amplifying the voltage at 34.5 kV. This resonant overvoltage caused the inverters to trip. Once offline, the resonance ceased and voltages returned to normal.

Additionally, transformer currents were found to be proportional to the harmonic voltage and exported to the grid, posing potential power quality concerns while the IBR remained online.

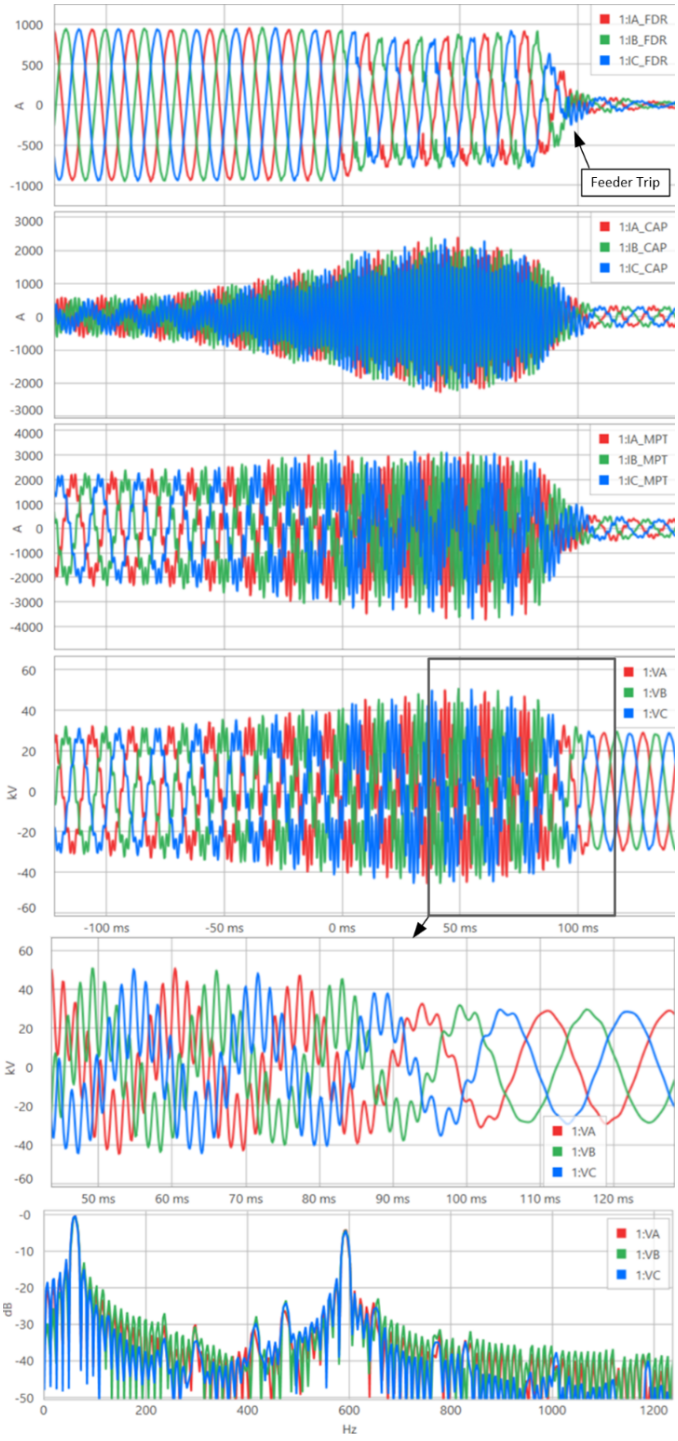

Fig. 54. Resonant harmonic overvoltage causes the inverter to trip

B. *Impairment of Negative-Sequence Line Current Differential Protection—August 2019*

High levels of harmonics and inter-harmonics can compromise the signal processing algorithms used in modern digital relays. Elements using I_2 are especially susceptible. This section shares a misoperation of the negative-sequence line current differential (87LQ) protection during normal operation.

Fig. 55 presents a field case in which there were significant current harmonics near 907 Hz (near the 15th harmonic) that led to the misoperation of a very-sensitively set 87LQ element [21]. The event occurred on a 0.2-mile, 138 kV line near a 184 MVA Type III wind facility during normal system conditions, demonstrating that harmonics can interfere with protection elements even in the absence of faults. Note that the reasons behind the high current harmonics are unknown. It is possible that it had a similar cause to the previous event described Section VIII.A.

To prevent recurrence of the 87LQ element trip, the utility desensitized the element's pickup setting, which has since addressed the misoperations. However, based on growing field experience, several utilities have opted to avoid using the 87LQ element altogether, especially on IBR-heavy circuits. Instead, they rely on:

- Phase current differential protection to detect phase faults and ground faults with modest resistance, and
- Zero-sequence current differential protection to add sensitive ground fault protection.

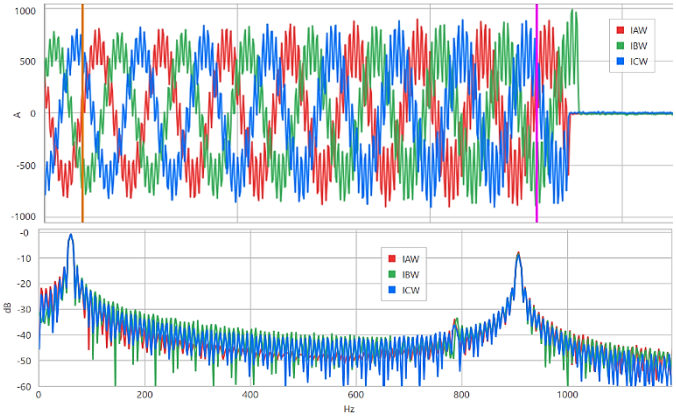

Fig. 55. Excessive current harmonics measured by a 138 kV line relay during normal operation

As IBR technology continues to mature and standardize, harmonic behavior is expected to improve. For example, IEEE Std 2800 Subclause 8.2.1 [2] places limits on current distortion from IBRs that are significantly lower than the levels observed in this event. Widespread adherence to such standards might improve the performance of protection functions like the 87LQ element.

C. *Differing Frequencies and Harmonics of Currents and Voltages—September 2023*

This event illustrates a case where negative-sequence directional protection (67Q1) experienced repeated, spurious assertions (referred to as chattering) in response to high harmonic current distortion under normal operating conditions.

Fig. 56 shows a simplified one-line diagram of three BESS facilities totaling 175 MW integrated into a 115 kV transmission network. Each facility connects through two stages of transformation: from the inverter output to 21.6 kV via an ungrounded inverter transformer, and from there to 115 kV via a step-up transformer. Due to the ungrounded connection at the inverter transformer, zero-sequence harmonic currents are blocked from flowing into the 21.6 kV bus.

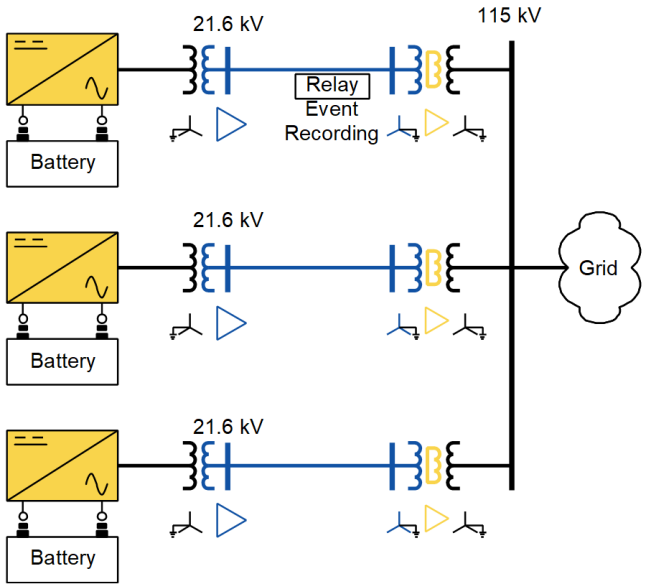

Fig. 56. Simplified one-line diagram showing the integration of three BESS facilities into a 115 kV transmission network

A sensitively set monitoring relay triggered an event report indicating the assertion of the negative-sequence directional element (67Q1), even though there was no external disturbance or abnormality in the system. The BESS facilities were operating normally.

Fig. 57 also displays the recorded three-phase current and voltage waveforms at the 21.6 kV bus. The current waveforms exhibited significant harmonic distortion, while the voltage waveforms did not appear as distorted.

A spectral analysis over a 200 ms window revealed the following:

- The fundamental frequency of the current waveforms was approximately 46.3 Hz, indicating potential control instability or waveform corruption.
- The voltage fundamental remained close to nominal at 59.73 Hz.
- A strong interharmonic component, 166.3 Hz, was present in the current spectrum (0 dB), and to a lesser extent in the voltage spectrum (–17.3 dB).

This mismatch between current and voltage fundamental frequencies can cause phasor misalignment and incoherency, leading to false directional assertions in elements like 67Q1. Furthermore, the presence of high interharmonic content compromises signal quality, making reliable direction detection difficult.

The event record shows the 67Q1 element briefly asserting near the end of the 100 ms snapshot. Over the full duration of the one-second recording (not shown), 67Q1 repeatedly picked up and dropped out, with each assertion lasting less than 10 ms, a classic signature of protection chattering caused by waveform distortion. A short time delay can help mitigate possible protection security challenges near IBRs.

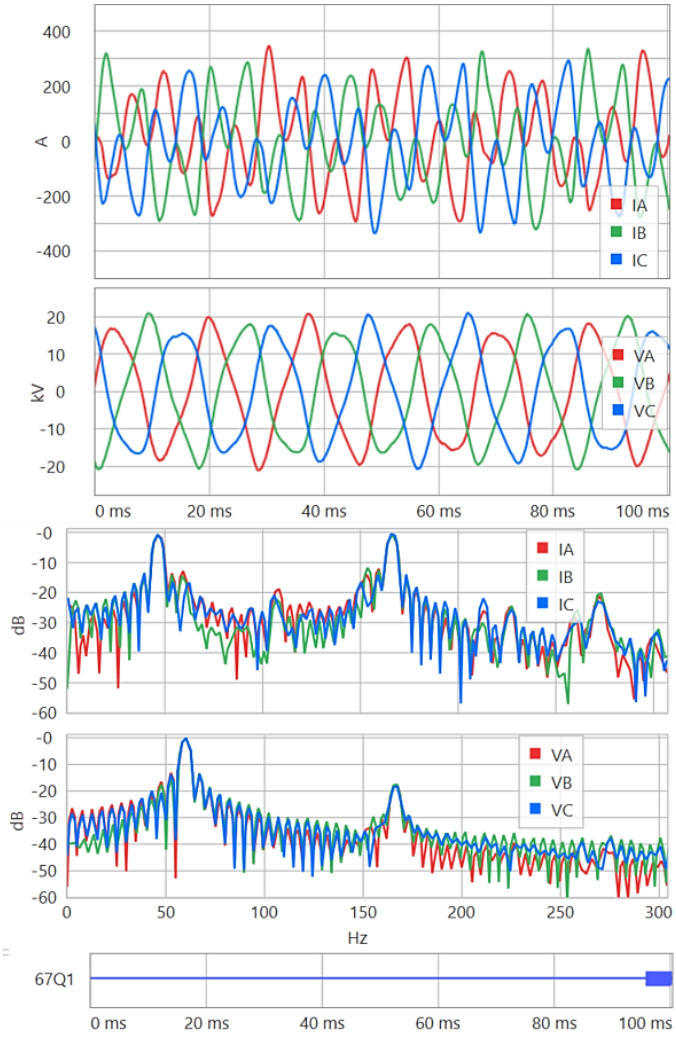

Fig. 57. Steady-state harmonic distortion recorded at the 21.6 kV bus of the BESS facility

D. Delayed Current Zeros and Controller Oscillations —January 2024

This event shows that the IBR fault response can have significant oscillations with large current dc offsets that result in missing current zeros. A protection trip due to missing current zeros can cause catastrophic breaker damage [22]. The fault currents also have significant harmonic content that causes protection elements to chatter and reduce dependability.

The oscillography in Fig. 58 is recorded by a line differential relay connected to a 230 kV line. It shows the fault response of the 225 MW solar facility connected to the 230 kV line. The fault was an out-of-zone Phase-A-to-B fault impacting a 115 kV line. As can be seen in the figure, there is a significant dc offset and prominent second harmonic content in the currents.

The entire record corresponding to the oscillography in Fig. 58 is shown in Fig. 59. In addition to the dc and harmonics discussed earlier, this oscillography shows subharmonic current oscillations, with each oscillation lasting approximately 100 ms. During the event, the nominal 230 kV voltage dropped to approximately 0.9 pu due to this external fault on the 115 kV line, indicating the fault was electrically remote. The assertion of the R87L digitals corresponds to the line differential element characteristic being in the restraint region. When the R87L bits deassert, as they do several times throughout the event, the line differential element could misoperate if the differential current is sufficiently high. In this event, the pickup was sufficiently high so that the differential element did not misoperate.

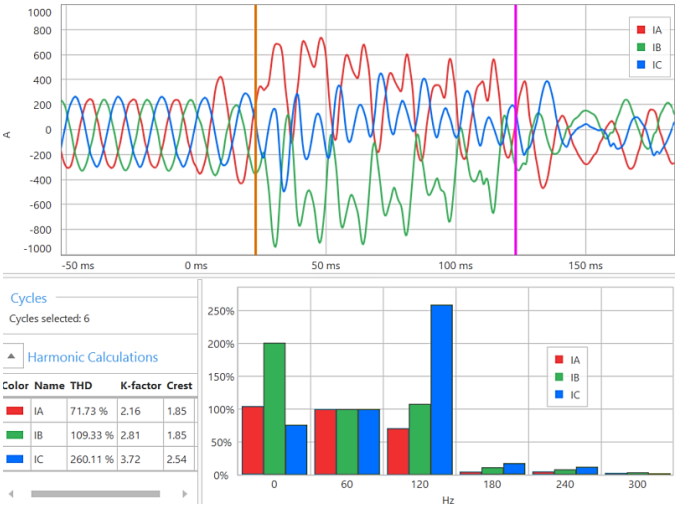

Fig. 58. Excessive dc and harmonics in fault currents for a remote Phase-A-to-B fault recorded on a 230 kV line

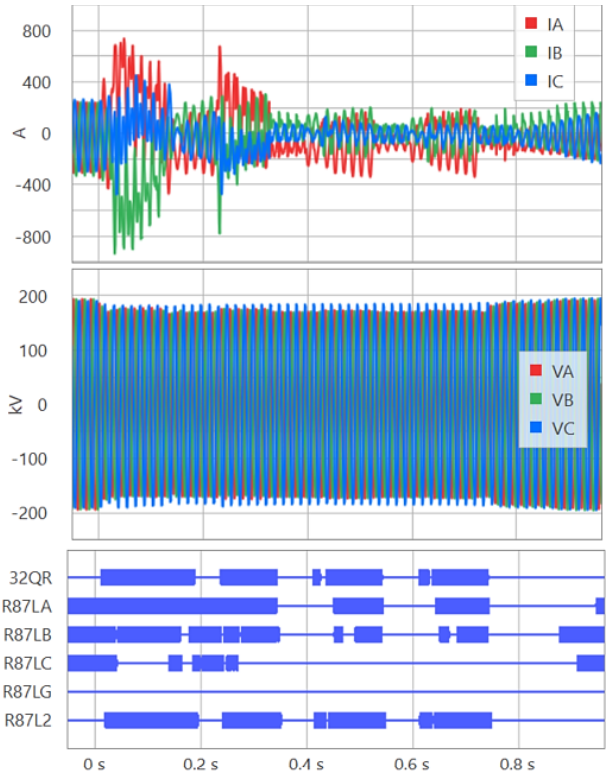

Fig. 59. Controller response captured by a 230 kV line relay for a remote AB fault

Reference [23] attributed these 100 ms time period oscillations in the current to the discontinuities from the deadband in the reactive power support characteristics of IBR, as per the WECC model shown in Fig. 60. When the reactive power support is not continuous by nature, it causes a sudden reactive current injection around the deadband boundaries, i.e.,

when delta voltages dV_1 or dV_2 are close to deadband boundaries in Fig. 60. For example, in Fig. 60, with a Slope $K_1 = dIq1/ dV1 = 2$, and $dV_{1max} = 0.1$ pu, there will be a sudden 0.2 pu current (dIq1) injection if dV1 slightly exceeds 0.1 pu. In contrast, if dV1 is slightly below 0.1 pu, there is no current injection. This causes a non-uniform response. Such behavior can be modeled in dynamic response simulations with oscillations showing a dc offset and second harmonics.

Some manufacturers have implemented the deadband in the reactive power support during a fault, as shown in Fig. 61 [23]. This deadband has hysteresis and prevents sudden current injections, which can help prevent oscillatory response.

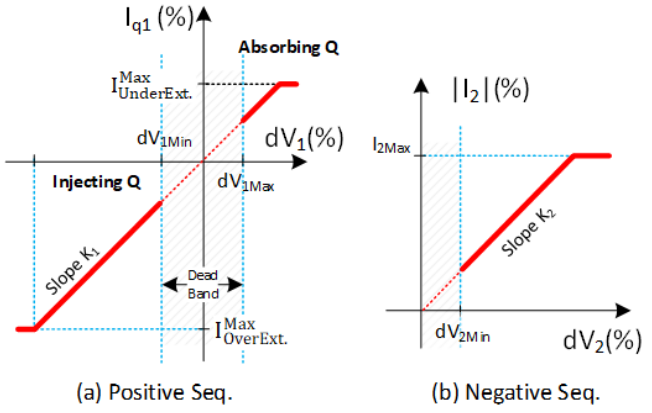

Fig. 60. Reactive power support injections band

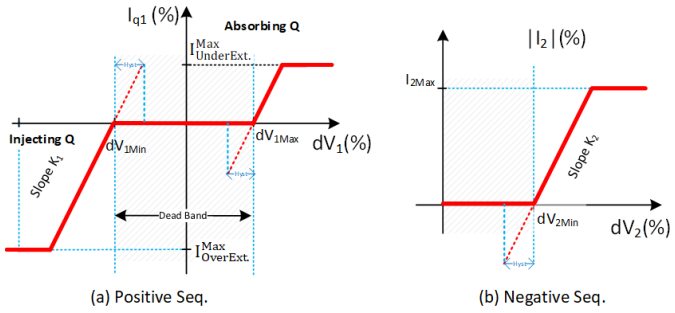

Fig. 61. Reactive power supports deadband and hysteresis

E. *Harmonics During Fault—December 2024*

The previous records in this section illustrate high harmonics during the steady-state and for a phase-to-phase fault. High harmonic content during ground faults are also quite common. The following event is from a 350 MW BESS and solar facility connected via a 230 kV line. Fig. 62 shows the oscillography for the remote Phase-C-to-ground fault. The fault was cleared with a typical three-cycle clearing time.

From Fig. 62, the zero-sequence current is clean, i.e., with a 60 Hz component. On the other hand, the IBR currents (with zero-sequence current removed) are noisy and have many harmonic and subharmonic components.

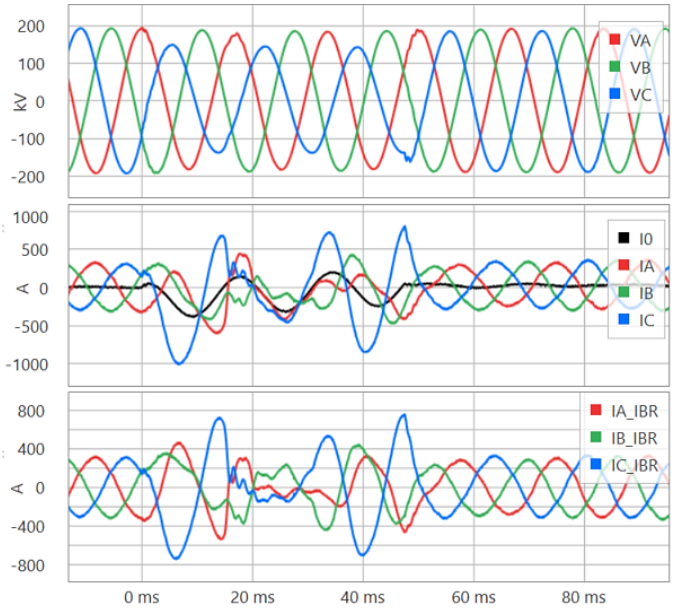

Fig. 62. Excessive harmonic content in currents from IBRs during a ground fault

Fault records from other events throughout this paper also illustrate this behavior, including the waveforms shown in Fig. 31 dating back to July 2000 near a Type III wind facility. Therefore, we note that this behavior has persisted for the past 25 years and is prevalent for both partial and full converter-interfaced IBRs.

F. *Key Observations and Risks*

This section presented five real-world events that underscore critical protection risks associated with IBRs.

The first event involved a resonant harmonic overvoltage trip, where the network at the collector bus was inadvertently tuned to the tenth harmonic (approximately 590 Hz). A very small injection of tenth-harmonic current from the IBR, less than 0.1 percent of the fundamental, resulted in significant overvoltage, ultimately causing the IBR to trip.

The next two events highlighted the vulnerability of negative-sequence protection schemes to harmonic distortion in IBR output currents. While line differential protection is generally considered dependable, excessive harmonic and inter-harmonic content can challenge digital filtering algorithms, particularly for negative-sequence differential elements, leading to an elevated risk of misoperation.

Modern grid codes increasingly require IBRs to provide both positive- and negative-sequence reactive current during voltage depressions, emulating the voltage support behavior of synchronous machines. However, one event revealed that deadband behavior in the reactive power control loop introduced waveform discontinuities and missing zero crossings. These irregularities in the current waveform could have contributed to circuit breaker failures if there was an unintended protection trip.

The remaining events showed that IBRs can inject significant harmonic content even during phase-to-phase faults. In one case involving a ground fault, the IBR current remained heavily distorted with pronounced harmonic and subharmonic components, particularly after zero-sequence current was filtered out. These distortions can cause protective relay digitals to chatter and potentially risk reliability of the protection system.

IX. IBR Controller Issues

The events in this section highlight not only the distinctive nature of short-circuit and post-fault responses in IBR systems, but also the challenges in explaining such behavior using conventional reasoning or physical principles, due to the opacity of proprietary control system logic.

A. Current Oscillations After Fault Clearing—March 2024

For the IBR facilities in Fig. 38, there were several events where all three phases of the currents oscillated post-fault. Fig. 63 shows the current oscillations for an external ground fault in the grid, which were recorded at the 230 kV line terminal.

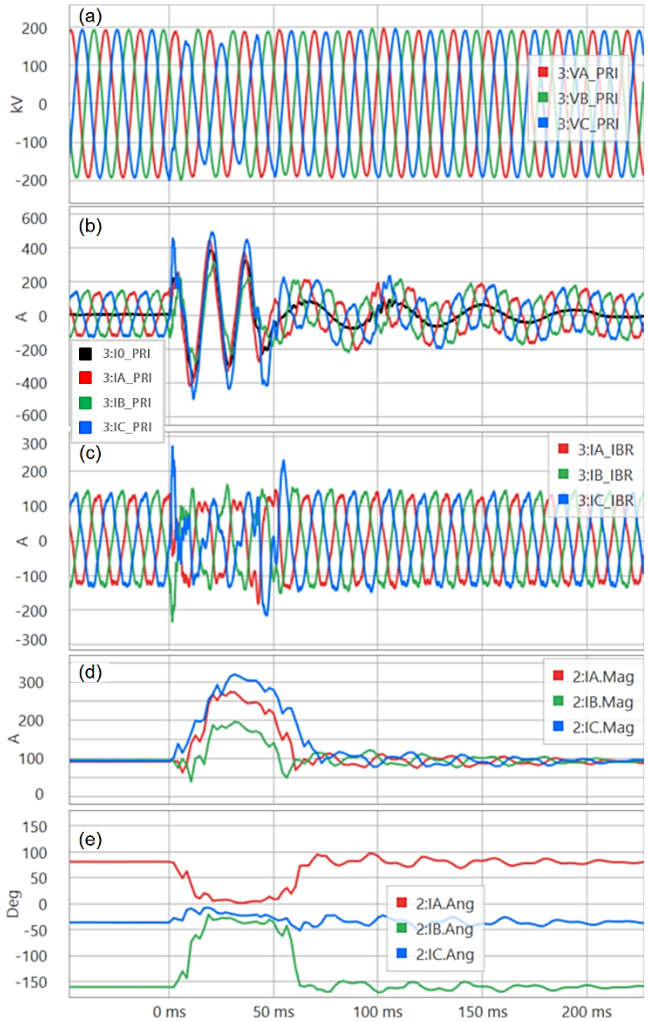

Fig. 63. Subsynchronous current oscillations after fault clearing

The external fault was cleared in 50 ms. Once the voltage returned to normal after the fault cleared, there were oscillations in the current output from the IBRs from 50 ms to 200 ms. The frequency of oscillation was 31 Hz. The COMTRADE record was played back through a line relay to observe the effects on the phasor measurements. The filtered current magnitude and angle are shown in Fig. 63(d) and Fig. 63(e), respectively. Because the current oscillation frequency occurs at half the nominal 60 Hz frequency, a portion of it leaks through the digital relay filter and results in the current magnitude and angle oscillations (see Fig. 44 for the attenuation provided by a typical one-cycle relay filter). The cause of the oscillations in the currents remains unknown at the time of publication.

B. Fault Current Changes Without Apparent Cause—March 2024

The unpredictable nature of IBRs is not limited to their differing responses across vendors or fault scenarios. Even a single inverter can exhibit significant variations in fault current during one fault event. This dynamic behavior adds another layer of complexity to accurately modeling and predicting inverter fault responses.

As shown in Fig. 64, a 148 MW BESS was connected to both the 115 kV and 230 kV networks via a short, 0.2-mile-long 115 kV gen-tie line. An adjacent 115 kV line experienced a Phase-C-to-ground fault, and DFR data were analyzed for both the faulted line and the gen-tie line.

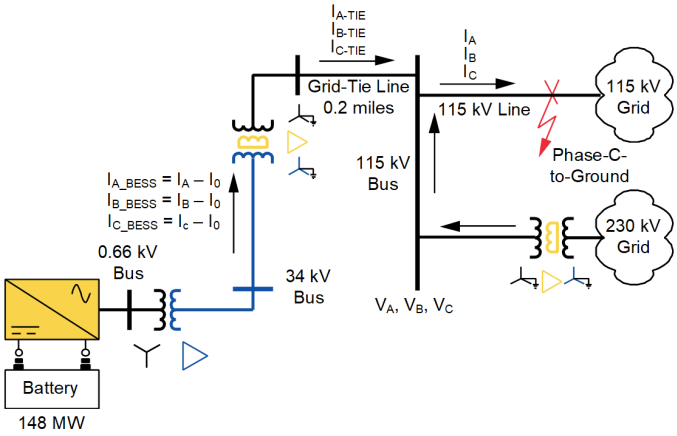

Fig. 64. Diagram of a 148 MW BESS connected to 115/230 kV system

Fig. 65 shows the record measured by the DFR and includes:

a. Three-phase currents in the faulted 115 kV line.
b. Three-phase currents in the 115 kV gen-tie line.
c. Three-phase voltages at the 115 kV gen-tie bus.

The faulted line current shown in Fig. 65(a) indicated that the remote end tripped in about 3 cycles, while the local end cleared the fault after approximately 24 cycles. Over this 24-cycle period, the gen-tie line current exhibited three distinct behavioral stages [14]:

- The **first three cycles** showed pronounced unbalance.
- The **next four cycles** resembled pre-fault load conditions.
- The **final 17 cycles** exhibited a new steady-state behavior.

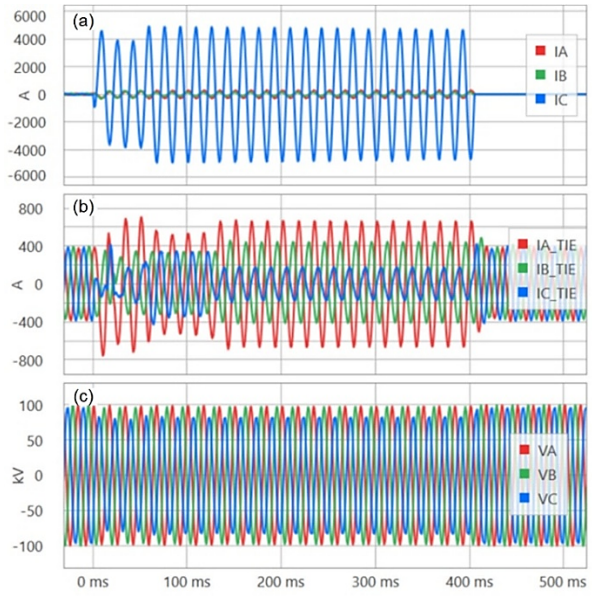

Fig. 65. Fault quantities measured by the DFR: a) phase currents from faulted line, b) phase currents from gen-tie line, and c) 115 kV DFR bus voltages

It is important to note that the 115 kV gen-tie line currents included an I_0 component resulting from the grounded-wye side of the 115/34.5/12 kV transformer. This component was absent on the inverter side (34.5 kV) and was thus removed to better reflect the actual inverter current contributions. After removing I_0 from the 115 kV gen-tie line current, the resulting three-phase currents, shown in Fig. 66, reflect the 34.5 kV currents from the IBR, except for their different magnitudes due to the transformer ratio. This removal provides a clearer picture of the actual currents supplied by the IBR on the 34.5 kV side during the fault.

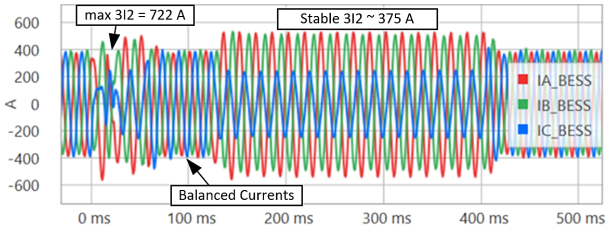

Fig. 66. 115 kV phase current after zero-sequence current removal showing significant IBR current changes without apparent cause

Some interesting phenomena can be observed from the gen-tie line currents in Fig. 66:

First three cycles:

1. The faulted phase (Phase C) exhibited distorted and suppressed current.
2. The unfaulted phases (A and B) had elevated current magnitudes.
3. A large and unstable negative-sequence current (I_2) was present.

Following four cycles:

1. All three phases showed balanced behavior.
2. Current magnitudes resembled pre-fault load levels.

Final 17 cycles:

1. The faulted phase continued with a reduced but stable current.
2. Unfaulted phases remained at elevated and steady levels.
3. A significant but now stable I_2 component persisted.

Pinpointing the exact causes of such a current pattern is challenging and requires a deep dive into the inverter's proprietary design and settings. One possible explanation is the changes of the 115 kV and 34.5 kV bus voltages when the remote end tripped shortly after three cycles. The voltages from Fig. 65(c) are magnified in Fig. 67. The voltage changes likely triggered IBR controllers to respond and change the current output. Although the 34.5 kV voltage was not recorded, it is reasonable to assume that it experienced similar changes to the 115 kV bus voltage.

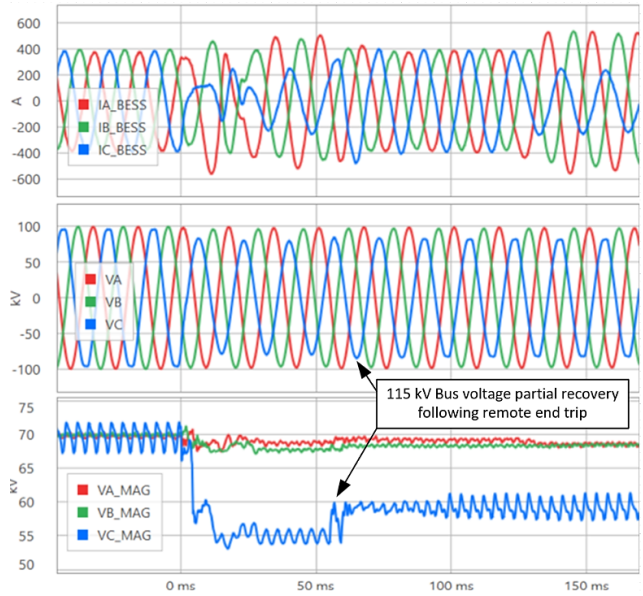

Fig. 67. 115 kV bus voltage change upon a remote-end trip

Unlike synchronous generators, the fault currents from IBRs depend on internal controls, which are proprietary designs and can be modified for various reasons. The variability in the currents shown in Fig. 66 makes it challenging to accurately model current IBRs.

C. Momentary Cessation Without Apparent Cause —January 2025

A subsequent event involving the BESS installation from Fig. 64 captured a puzzling control behavior: IBR repeatedly entered momentary cessation during an external fault, without any apparent triggering condition. Fig. 68 shows the BESS response to an external Phase-C-to-ground fault that is cleared in 1.1 seconds by the adjacent line protection.

At the fault inception, the IBR initially responded to an unbalanced voltage by injecting unbalanced currents as anticipated. However, rather than maintaining a steady contribution, the inverter exhibited erratic behavior by alternating among:

- Injecting unbalanced fault currents,
- Reverting to balanced, pre-fault-like currents, and
- Entering momentary cessation, during which current injection was interrupted.

This sequence of transitions occurred multiple times over the 1.1-second fault duration, demonstrating a lack of consistent control strategy or fault ride-through behavior.

The IBR had a rated current of 662 A and a measured pre-fault current of 656 A. During the fault, the current reached a maximum of 874 A (or 1.32 pu of rated current). This was the only observed case at this facility in which the IBR injected more than 1.2 pu of current during a fault. The event suggests a correlation between pre-fault operating conditions and fault current injection capability. Specifically, when the BESS operates near its rated output, it appears capable of momentarily injecting up to 1.3 pu during a fault.

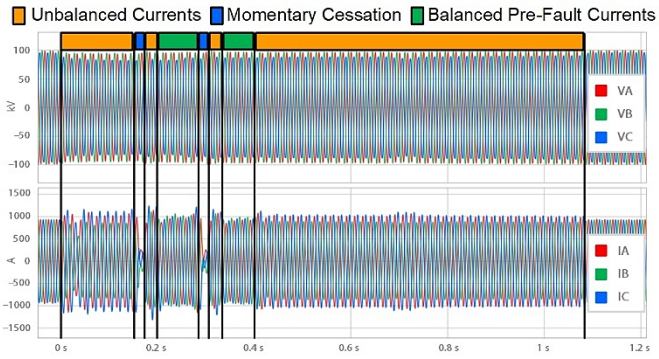

Fig. 68. Momentary cessation due to controller issue, providing inconsistent response during fault

D. Key Observations and Challenges

The events presented in this section revealed several critical challenges in understanding and protecting IBRs. These challenges stem largely from the opaque, proprietary nature of their control systems, which are driven by internal firmware logic. This lack of transparency hinders protection engineers from fully understanding or predicting IBR behavior during system disturbances.

In the first event from March 2024, post-fault current oscillations at subsynchronous frequencies were observed. Although these oscillations lasted less than 200 ms, they introduced phasor instability and affected relay performance due to the limitations of digital filtering algorithms. The cause appears to be rooted in internal controller dynamics, but without access to the inverter's design logic, it remains speculative.

The second (March 2024) event illustrated that even the same inverter can exhibit unpredictable behavior during a single fault. The faulted-phase current showed distortion and attenuation at inception, followed by a significant stable evolving negative-sequence contribution after the fault. These variations challenge the reliability of negative-sequence-based protection and highlight the impracticality of deriving countermeasures without visibility into proprietary inverters that are difficult to predict and model.

A third event demonstrated erratic behavior in response to an external ground fault, where the BESS alternated between injecting unbalanced fault currents, normal pre-fault-level currents, and momentary cessation. This inconsistency undermines protection dependability and suggests sensitivity to operating conditions, such as inverter loading or controller thresholds for ride-through and disconnection.

X. Summary of Field Events

The paper includes many utility field events that illustrate the different current challenges in IBR applications. To aid the reader, the events are indexed and cross-referenced in Table I.

Table I
Summary of Field Events

Section #	Event Date	IBR Type	MW	Figure	Fault Type and Notes
IV.A.1	August 2014	Type III	310	Fig. 10	BG -> BCG. I2 leads V2 by 155 degrees. Loss of 32Q dependability. BG fault misidentified as AG.
IV.A.2	August 2020	Type III	99	Fig. 13	CG. I2 leads V2 by 130 degrees. I2 > I1.
IV.A.3	March 2022	Type III	575	Fig. 15	CA. Phase-to-phase voltages do not reflect fault type. Phase Mho Zone 1 transient overreach.
IV.B.1	June 2021	Solar + BESS	160	Fig. 17	AG. Loss of 32Q security.
IV.B.2	January 2024	Solar	150	Fig. 19	AG. Loss of 32Q security.
IV.B.3	March 2021	Solar	145	Fig. 21	AG. Fault misidentified as CG.
IV.B.4	March 2022	Solar	30	Fig. 23	AG. Loss of 32Q security leads to POTT scheme misoperation.
IV.C	October 2023	Type III	24	Fig. 25	AB -> ABC. Phase mho Zone 1 overreaches for uncleared (~500 ms) fault.
IV.D.1	May 2024	Solar	225	Fig. 28	ABC. LOP due to low three-phase fault current contribution.
IV.D.2	July 2018	Type IV	102	Fig. 29	ABC. LOP due to cease mode response for three-phase fault.
IV.E	July 2000	Type III	NA	Fig. 31	CG. GFL IBR remains energized during reclosing.
V.A	October 2018	Type IV	102	Fig. 33	CA. GFL IBR attempts to energize the line. Narrow miss of out-of-sync closing.
V.B	August 2020	Solar + BESS	194	Fig. 35	BG. Facility 1 (ride-through) differs response from Facility 2 (cessation).
V.C	April 2024	Solar + BESS	350	Fig. 37	BG. Cessation not evident from phase currents.

Section #	Event Date	IBR Type	MW	Figure	Fault Type and Notes
V.D.1	June 2024	Solar + BESS	112	Fig. 39	AG. Different behavior of the same IBR during reclosing.
V.D.2	February 2024	Solar + BESS	112	Fig. 40	AG. IBR injects reduced fault current relative to capability.
VI.A	October 2022	Solar	6	Fig. 42	CG. Loss of overvoltage element dependability due to ROCOF > 60 Hz/s.
VI.B	May 2025	Solar	10	Fig. 46	CG. High ROCOF causes unexpected operating time delays.
VII.A	August 2024	BESS	400	Fig. 48	BG. Transformer overexcitation when IBR boosts voltage and reduces frequency for three seconds disconnecting from grid.
VII.B	September 2017	Type III	280	Fig. 50	BG. Southern Texas SSO with 2.45 pu voltage. Transformer differential misoperation due to overexcitation at 25 Hz.
VII.C	July 2025	Solar	300	Fig. 52	Unknown trigger. Forced SSO, control interactions between solar and STATCOM.
VIII.A	March 2025	Solar	250	Fig. 54	No fault. Resonant overvoltage at 590 Hz causes inverter trip.
VIII.B	August 2019	Type III	163	Fig. 55	No fault. Harmonics at 907 Hz causes 87LQ misoperation.
VIII.C	September 2023	BESS	175	Fig. 57	No fault. Difference between current and voltage fundamental frequencies. High harmonics at 166 Hz.
VIII.D	January 2024	Solar	225	Fig. 58	AB. Delayed current zeros. Controller oscillations and discontinuities in reactive power support due to lack of hysteresis.
VIII.E	December 2024	BESS + Solar	352	Fig. 62	CG. Fault with significant harmonics.
IX.A	March 2024	Solar + BESS	112	Fig. 63	CG. ~30 Hz current oscillations after fault clearing.
IX.B	March 2024	BESS	148	Fig. 65	CG. IBR control changes fault clearing.
IX.C	January 2025	BESS	148	Fig. 68	CG. IBR control goes in and out of cessation.

XI. Conclusions

This paper presented approximately 30 field-recorded events spanning 25 years of IBR integration into utility grids. These events collectively demonstrate that, unlike synchronous machines, IBRs (particularly those with a full converter interface) exhibit highly non-deterministic responses, not only during short-circuit conditions but also during steady-state operations and other common system events. Protection philosophies rooted in synchronous generator behavior are increasingly challenged as the grid transitions to a high-IBR environment.

The following insights are applicable to full converter IBRs, unless explicitly stated as Type III WTGs:

- **Negative-sequence protection** performance is impaired by distorted and phase-shifted current contributions from IBRs. Type III wind turbines, for instance, were observed injecting I_2 that led V_2 by as much as 155 degrees, compromising directional element dependability and faulted phase identification. Full converter IBRs often inject minimal I_2 with variable frequencies and phase angles in all quadrants, further impairing security of the protection systems.
- **Inconsistent I_2–V_2 and I_2–I_0 phase angle** relationships can result in incorrect directional decisions and misidentification of the faulted phase.
- **Memory-polarized phase distance elements become unstable** for full-converter or Type III WTGs due to corruption of the positive-sequence memory voltage at IBR terminals and oscillations in calculated apparent impedance, leading to transient overreach and unpredictable relay zone reach.
- **Momentary or partial cessations** can limit IBR short-circuit current contributions to well below the assumed 1.0–1.3 pu range, undermining both relay dependability and coordination with remote terminals.
- **Extended cessation** poses a risk of out-of-sync closing on the IBR tie line equipped with autoreclosing.
- **Loss-of-potential (LOP) logic** may be incorrectly picked up and remain latched, particularly for multiphase faults, compromising protection reliability.
- **Digital relay filtering** techniques, developed for high-inertia systems, may misoperate in low-inertia IBR networks due to rapid frequency shifts, filtering lag, and timing inconsistencies tied to frequency deviation.
- **Discontinuities in reactive current support** from IBR controllers can lead to missing current zero-crossings, raising the risk of breaker failure if protection is not properly delayed.
- **Transformer overexcitation** can occur during slow shutdown of islanded IBRs unless volts-per-hertz protection is applied, an important lesson from synchronous generator protection that remains relevant.
- **Voltage instability and oscillatory behavior** may result from the dynamic interaction of multiple inverter controllers, as seen in one event involving a solar plant and a nearby STATCOM. These interactions caused significant power swings and

degraded power quality, even under strong grid conditions.

- **SSO risks** are present when Type III WTGs operate radially into series-compensated lines, highlighting the need for proactive mitigation via detection schemes, bypass controls, or generator tripping logic. Forced SSO may also occur for full converter-interfaced IBRs that can significantly degrade power quality and present risk to equipment.

These findings highlight a significant gap between traditional protection design and the dynamic, firmware-driven behavior of IBRs. Protection elements that are practically independent of source characteristics—current differential and zero-sequence-based elements—remain reliable but are not universally applied. Unless protection strategies are fundamentally rethought to reflect the unique characteristics of IBRs, protection reliability remains vulnerable. Furthermore, some risks cannot be fully mitigated without increased transparency into proprietary IBR control designs.

A coordinated response is essential. Progress depends on collaboration across multiple domains:

- **IBR manufacturers** should work toward standardized, transparent short-circuit current responses.
- **Regulators** must reinforce grid codes (e.g., IEEE Std 2800, NERC PRC-024/025/029) requiring consistent ride-through performance and reactive current support during abnormal voltage conditions.
- **Relay manufacturers** must innovate protection schemes that account for low fault current levels, non-synchronous sequence behavior, and fast controller dynamics.
- **Protection engineers** must adapt by updating coordination studies, validating response assumptions, and leveraging advanced tools such as synchrophasor-based detection and adaptive relay logic.

The path to a reliable, IBR-dominated grid demands multidisciplinary collaboration, field insight, regulatory leadership, and a deeper integration of control system behavior into protection designs.

XII. Acknowledgments

The authors thank Michael Jensen, Brett Cockerham, Scott Elling, Bernard Matta, Ryan McDaniel, Prabin Adhikari, and Normann Fischer for their careful technical reviews and thoughtful comments. They are also grateful to Sanan Kolva for her editorial review, which improved the quality of this paper.

XIII. References

[1] VDE-AR-N 4130, "Technical Requirements for the Connection and Operation of Customer Installation to the Extra High Voltage Network (TAR Extra High Voltage)," November 2018.

[2] IEEE Std 2800-2022, IEEE Standard for Interconnection and Interoperability of Inverter-Based Resources (IBRs) Interconnecting with Associated Transmission Electric Power Systems, April 2022.

[3] M. Nagpal and C. Henville, "Impact of Power-Electronic Sources on Transmission Line Ground Fault Protection," *IEEE Transactions on Power Delivery*, Vol. 33, Issue 1, February 2018, pp. 62–70.

[4] K. Zimmerman and D. Costello, "Fundamentals and Improvements for Directional Relays," proceedings of the 63rd Annual Conference for Protective Relay Engineers, TX, March 2010.

[5] D. Costello and K. Zimmerman, "Determining the Faulted Phase," proceedings of the 36th Annual Western Protective Relay Conference, Spokane, WA, October 2009.

[6] B. Kasztenny, B. Campbell, and J. Mazereeuw, "Phase Selection for Single-Pole Tripping – Weak Infeed Conditions and Cross-Country Faults," proceedings of the 27th Annual Western Protective Relay Conference, Spokane, WA, October 2000.

[7] R. Chowdhury and N. Fischer, "Transmission Line Protection for Systems With Inverter-Based Resources – Part I: Problems," in *IEEE Transactions on Power Delivery*, Vol. 36, Issue 4, August 2021, pp. 2416–2425.

[8] E. O. Schweitzer, III and J. Roberts, "Distance Relay Element Design," proceedings of the 19th Annual Western Protective Relay Conference, Spokane, WA, October 1992.

[9] H. Mohammadpour, A. Banaiemoqadam, A. Hooshyar, and A. Al-Durra, "Eliminating the Need for a Less Strict Requirement for the Negative-Sequence LVRT Current of Type-III Wind Turbine Generators in the IEEE 2800 Standard," in *IEEE Transactions on Sustainable Energy*, Vol. 14, Issue 1, January 2023, pp. 587–601.

[10] J. E. Beehler, "Weather, Corona, and the Decay of Trapped Energy on Transmission Lines," in *IEEE Transactions on Power Apparatus and Systems*, Vol. 83, Issue 5, May 1964, pp. 512–520.

[11] NERC PRC-029-1, Frequency and Voltage Ride-through Requirements for Inverter-based Resources, 2025.

[12] IEEE Std 1547-2018, IEEE Standard for Interconnection and Interoperability of Distributed Energy Resources with Associated Electric Power Systems Interfaces, April 2018.

[13] M. Nagpal, F. P. Plumptre, R. Fulton, and T. Martinich, "Dispersed generation interconnection–utility prospective," *IEEE Transactions on Industry Applications*, Vol. 42, Issue 3, May 2006, pp. 864–872.

[14] D. Zhang, "Event Analysis: Innovative Tools and Strategies for Protection Engineers," proceedings of the 51st Annual Western Protective Relay Conference, Spokane, WA, October 2024.

[15] GE Energy, "Generator Protection," General Electric Company, GEK 7512l, revised August 2009, p.13.

[16] Y. Cheng et al., "Wind Energy Systems Sub-Synchronous Oscillations: Events and Modeling," in *IEEE Power & Energy Society*, PES-TR80, July 2020.

[17] M. Nagpal et al., "Protection Challenges and Practices for Interconnecting Inverter Based Resources to Utility Transmission Systems," in *IEEE Power & Energy Society*, PES-TR81, July 2020.

[18] NERC, Recommended Oscillation Analysis for Monitoring and Mitigation Reference Document, November 2021.

[19] NERC Reliability Guideline, Forced Oscillation Monitoring and Mitigation, September 2017.

[20] IEEE Std C37.106-2022, IEEE Guide for Abnormal Frequency Protection for Power Generating Plants, May 2023.

[21] R. Chowdhury, R. McDaniel, and N. Fischer, "Line Current Differential Protection in Systems With Inverter-Based Resources—Challenges and Solutions," proceedings of the 49th Annual Western Protective Relay Conference, Spokane, WA, October 2022.

[22] M. Nagpal, K. Hadzimahovic, T. Scott, T. Jiao, R. Barone, F. Calero, and R. Chowdhury, "Catastrophic Breaker Failures Due to Missing Current Zero-Crossings in Highly Shunt-Compensated 500 kV Lines—Point-on-Wave, Reclosing, and Protection Considerations," proceedings of the 50th Annual Western Protective Relay Conference, Spokane, WA, October 2023.

[23] A. Saeed, M. Jensen, M. Reno, A. Bidram, and A. Zamani, "Utilities Perspective on Protection Challenges with High IBR Penetration," Pacific Gas Electric Company, San Francisco, CA, Technical Report, September 2024.

XIV. BIOGRAPHIES

Mukesh Nagpal is a Senior Associate Technical Consultant at Burns & McDonnell and an IEEE Fellow. With over 35 years of experience in electric utility research and power system protection, Mukesh has made notable contributions to the economic, safe, and reliable integration of renewables into the electric grid. He has published approximately 50 technical papers showcasing his expertise in this field.

Ajmal Saeed is a Principal Protection Engineer for Pacific Gas and Electric Company in Sacramento, CA. He earned his MS in Electrical Engineering from Rensselaer Polytechnic Institute, NY and BS from the University of Engineering and Technology, Lahore, Pakistan. His areas of interest include protection systems, electrical design, electric system modeling and engineering applications for the utility industry. He can be reached at: Ajmal.Saeed@pge.com.

Ricardo Rangel received his BSEE from California State University, Fresno and MSEE from University of California, Los Angeles. He is a registered Professional Engineer in the State of California and currently works as a System Protection Engineer at Pacific Gas and Electric Company in Fresno, CA supporting the transmission system for 230 kV and below. His area of interest is power system impedance calculations using relay data and he has authored several technical papers on this topic.

Daniel Zhang is a is currently an Expert Protection Engineer with Pacific Gas and Electric (PG&E) based in San Ramon, CA. He supports PG&E's 500 kV System Protection, Remedial Action Scheme, Phasor Measurement Units, etc. He received his BSc and MSc degrees in 1993 and 1996, respectively, from Xi'an Jiaotong University, Xi'an China, and MESc in 2003 from University of Western Ontario, London, Ontario, Canada. He has been working in the field of power system protection and control for over 20 years with utilities and engineering firms. He is a registered professional engineer in NY State.

Ritwik Chowdhury received his BS degree in engineering from the University of British Columbia and his MS degree in engineering from the University of Toronto. He joined Schweitzer Engineering Laboratories, Inc. (SEL) in 2012, where he is presently a principal engineer in research and development. Ritwik holds over 15 patents and has coauthored over 35 technical papers. He was recognized as an exceptional reviewer for *IEEE Transactions on Power Delivery* for three years. He is a past chair of the Protection and Control Practices Subcommittee (I-SC) of the IEEE Power System Relaying and Control (PSRC) Committee and the recipient of the 2021 PSRC Outstanding Young Engineer Award. Ritwik is a senior member of IEEE, a member of CIGRE, and a registered professional engineer in the province of Ontario.